National Library of Canada
Bibliothèque nationale du Canada

Canadian Theses Service
Service des thèses canadiennes

Ottawa, Canada
K1A 0N4

NOTICE

The quality of this microform is heavily dependent upon the quality of the original thesis submitted for microfilming. Every effort has been made to ensure the highest quality of reproduction possible.

If pages are missing, contact the university which granted the degree.

Some pages may have indistinct print especially if the original pages were typed with a poor typewriter ribbon or if the university sent us an inferior photocopy.

Reproduction in full or in part of this microform is governed by the Canadian Copyright Act, R.S.C. 1970, c. C-30, and subsequent amendments.

AVIS

La qualité de cette microforme dépend grandement de la qualité de la thèse soumise au microfilmage. Nous avons tout fait pour assurer une qualité supérieure de reproduction.

S'il manque des pages, veuillez communiquer avec l'université qui a conféré le grade.

La qualité d'impression de certaines pages peut laisser à désirer, surtout si les pages originales ont été dactylographiées à l'aide d'un ruban usé ou si l'université nous a fait parvenir une photocopie de qualité inférieure.

La reproduction, même partielle, de cette microforme est soumise à la Loi canadienne sur le droit d'auteur, SRC 1970, c. C-30, et ses amendements subséquents.

NL-339 (r. 88/04) c

Canada

UNIVERSITY OF ALBERTA

THE MEASUREMENT OF OXYGEN PRESSURE OF MOLTEN SUBMERGED ARC WELDING FLUXES USING DISPOSABLE OXYGEN PROBES.

BY

ALLISON HARDY

A THESIS

SUBMITTED TO THE FACULTY OF GRADUATE STUDIES AND RESEARCH IN PARTIAL FULFILLMENT OF THE REQUIREMENTS FOR THE DEGREE OF MASTER OF SCIENCE

IN

METALLURGICAL ENGINEERING

DEPARTMENT OF MINING, METALLURGICAL AND PETROLEUM ENGINEERING

EDMONTON, ALBERTA

FALL 1991

National Library of Canada
Bibliothèque nationale du Canada

Canadian Theses Service
Service des thèses canadiennes

Ottawa, Canada
K1A 0N4

The author has granted an irrevocable non-exclusive licence allowing the National Library of Canada to reproduce, loan, distribute or sell copies of his/her thesis by any means and in any form or format, making this thesis available to interested persons.

L'auteur a accordé une licence irrévocable et non exclusive permettant à la Bibliothèque nationale du Canada de reproduire, prêter, distribuer ou vendre des copies de sa thèse de quelque manière et sous quelque forme que ce soit pour mettre des exemplaires de cette thèse à la disposition des personnes intéressées.

The author retains ownership of the copyright in his/her thesis. Neither the thesis nor substantial extracts from it may be printed or otherwise reproduced without his/her permission.

L'auteur conserve la propriété du droit d'auteur qui protège sa thèse. Ni la thèse ni des extraits substantiels de celle-ci ne doivent être imprimés ou autrement reproduits sans son autorisation.

ISBN 0-315-70188-9

Canada

UNIVERSITY OF ALBERTA

RELEASE FORM

NAME OF AUTHOR: ALLISON HARDY

TITLE OF THESIS: THE MEASUREMENT OF OXYGEN PRESSURE OF MOLTEN SUBMERGED ARC WELDING FLUXES USING DISPOSABLE OXYGEN PROBES

DEGREE: MASTER OF SCIENCE

YEAR THIS DEGREE GRANTED: 1991

Permission is hereby granted to the University of Alberta Library to reproduce single copies of this thesis and to lend or sell such copies for private, scholarly or scientific research purposes only.

The author reserves all other publication and other rights in association with the copyright in the thesis, and except as hereinbefore provided neither the thesis nor any substantial portion thereof may be printed or otherwise reproduced in any material form whatever without the author's prior written permission.

Allison Hardy

ALBERTON R.R.#2

P.E.I., CANADA

DATE: Oct 11, 1991

UNIVERSITY OF ALBERTA

FACULTY OF GRADUATE STUDIES AND RESEARCH

The undersigned certify they have read, and recommend to the Faculty of Graduate Studies and Research for acceptance, a thesis entitled THE MEASUREMENT OF OXYGEN PRESSURE OF MOLTEN SUBMERGED ARC WELDING FLUXES USING DISPOSABLE OXYGEN PROBES submitted by ALLISON HARDY in partial fulfillment of the requirements for the degree of MASTER OF SCIENCE in METALLURGICAL ENGINEERING.

Dr. B.M. Patchett

Dr. J.M. Whiting

Dr. S.A. Bradford

Dr. I.D. Sommerville

Date: Oct 9/91

ABSTRACT

Oxygen probes have been used extensively to measure the dissolved oxygen content in liquid metals. A more recent application of oxygen probes has been to measure the oxygen pressure in steelmaking slags. They have been used successfully to determine oxide activities in complex slag mixtures.

An extension of this technology was to measure the oxygen pressure in molten Submerged Arc Welding (SAW) fluxes. The oxygen pressure of SAW fluxes is a direct measurement of the potential of the flux to give up oxygen to the weld metal. A low oxygen pressure flux is required for producing low oxygen content welds. This improves the mechanical properties of the weld, especially the weld metal fracture toughness.

A needle type oxygen probe was developed for the rapid determination of oxygen pressure in molten SAW fluxes. It was constructed by plasma spraying a solid electrolyte on to a molybdenum wire. Yttria doped zirconia was used as a solid electrolyte which conducts only oxygen anions. The molybdenum wire was oxidized to provide the reference oxygen pressure by the Mo/MoO_2 equilibrium reaction.

The oxygen pressure was measured in five fluxes of compositions varying from highly acid to mildly basic. With the use of a special vertical tube furnace and a crucible made from zirconia grain stabilized platinum,

measurements were taken up to 1600 °C. The voltage readings from the probes typically stabilized in 30 to 90 seconds. Stable voltages were measured for 30 to 60 second when either the probe was removed or it deteriorated in the molten flux.

It was determined from the results of the oxygen probe measurements that the oxygen pressure (pO_2) increased with temperature and the ln pO_2 varied linearly with the inverse of the temperature. The slope of this relationship was generally higher for the fluxes with lower pO_2 although the two MnO-SiO_2 based fluxes had similar pO_2 measurements but very different slopes.

The pO_2 measured in this study correlated with the optical basicity of the fluxes at steelmaking temperatures (1600 °C). This correlation did not hold for higher or lower temperatures. There was no correlation between the Basicity Index recommended by the International Institute of Welding and the pO_2 of the fluxes.

Finally, a statistical relationship between the ln pO_2 and the chemistry of the flux was determined, as well as the effects of temperature. An excellent correlation was found between the ln pO_2 and the molar percentages of CaF_2, CaO, MnO and SiO_2 of the flux.

ACKNOWLEDGEMENTS

The author sincerely wishes to thank Dr. Barry Patchett for his supervision and guidance throughout my graduate studies at the University of Alberta. A special thanks also goes to Dr. Tom Etsell for providing expert advice.

The author wishes to thank the Alberta Research Council for plasma spraying the solid electrolyte material to make the oxygen probes.

Finally, the author's thanks go to NSERC for providing funding so that this graduate research was possible.

TABLE OF CONTENTS

		PAGE
CHAPTER I		1
A.	Introduction	1
B.	The Submerged Arc Welding Process	4
C.	Importance of Oxygen in Weld Metal	7
D.	Sources of Oxygen	10
CHAPTER II		13
A.	Structure of Silicate Melts	13
B.	Basicity	16
C.	Basicity Ratios	19
D.	Optical Basicity	21
E.	Oxygen Potential	24
F.	Estimation of Weld Metal Oxygen	27
G.	Oxygen Pressure of Slags	31
CHAPTER III		33
A.	Ionic Conduction	33

B. Oxygen Concentration Cells 36
C. Electronic Conduction 39
D. Disposable Oxygen Concentration Cells 41
E. Some Applications of Oxygen Probes 46

CHAPTER IV 50

A. Probe Design 50
B. Furnace Design 52
C. Experimental Procedure 53

CHAPTER V 55

A. $ZrO_2(CaO)$ vs. $ZrO_2(Y_2O_3)$ Solid Electrolyte 55
B. Results 58
C. Discussion 65
D. Conclusion 76

REFERENCES 113
APPENDICES 116

LIST OF TABLES

		PAGE
1.	Examples of some Basicity Ratios of slags used in steelmaking	78
2.	Relationship between Fe^{2+}/Fe^{3+} and oxygen pressure of sodium disilicate glass	79
3.	Plasma spray parameters for application of $ZrO_2(Y_2O_3)$	80
4.	Composition of solid electrolytes	81
5.	Composition of the Submerged Arc Welding fluxes	82
6.	Calculated ln pO_2 values from EMF reading of the oxygen probes	83
7.	Theoretical percent oxygen in iron if it is melted with an equal volume of flux	84

LIST OF FIGURES

		PAGE
1.	Schematic of SAW process.	85
2.	Typical Charpy V-notch toughness and weld metal oxygen content for different flux types.	86
3.	Cooling curve for a low carbon, low alloy steel showing the effects of oxygen content. M=Martensite, AC=Aligned ferrite with carbide (upper bainite), AF=Acicular ferrite and BF=Blocky ferrite.	87
4.	Typical oxygen and nitrogen content of weld metal for different welding processes.	88
5.	Structure of a) crystalline and b) molten silica.	89
6.	Theoretical concentration of bridging (O^0), non-bridging (O^{1-}) and free (O^{2-}) oxygen for different values of the equilibrium constant (K).	90
7.	Basicity Index (IIW) versus weld metal oxygen content. a) without CaF_2 term b) with CaF_2 term.	91
8.	Dissolved oxygen equilibrium based on the SiO_2 and the Fe_xO reactions as a function of basicity for SiO_2-CaO-FeO slags.	92
9.	Schematic of an oxygen concentration cell.	93
10.	Ionic conduction of different solid electrolytes as a function of percent anion vacancies.	94
11.	Common types of oxygen probes. (a)Tube type (b)Plug type and (c)Needle type.	95
12.	Oxidation state of iron as a function of basicity.	96
13.	Schematic of needle probe used in this study.	97
14.	Schematic of furnace used in this study.	98
15.	Cross section of used ZrO_2(CaO) probe.	99

16. Cross section of used $ZrO_2(Y_2O_3)$ probe 100

17. ln pO2 versus 1/temperature 101

18. Oxygen probe's EMF response for flux #20 using the $ZrO_2(CaO)$ probes 102

19. Oxygen probe's EMF response for flux #20 using the $ZrO_2(Y_2O_3)$ probes 103

20. Oxygen probe's EMF response for flux #1 using the $ZrO_2(Y_2O_3)$ probes 104

21. Oxygen probe's EMF response for flux #3 using the $ZrO_2(Y_2O_3)$ probes 105

22. Oxygen probe's EMF response for flux #4 using the $ZrO_2(Y_2O_3)$ probes 106

23. Oxygen probe's EMF response for flux #50 using the $ZrO_2(Y_2O_3)$ probes 107

24. Oxygen probe's EMF response for flux #91 using the $ZrO_2(Y_2O_3)$ probes 108

25. ln pO_2 versus 1/temperature, extrapolated to 2600 K 109

26. ln pO_2 versus Basicity Index (IIW) at various temperatures 110

27. ln pO_2 versus Optical Basicity at various temperatures 111

28. ln pO_2 versus theoretical percent oxygen in the weld metal using the method for calculations from Eagar (ref. 6) 112

CHAPTER I

A. INTRODUCTION

The technology of joining metals has been one of the most important and rapidly developing fields in metallurgy. The current state of knowledge in welding has been deeply rooted in the evolution of the welding processes themselves. Industrial experience was the leading source of information as to the capabilities and limits of the welding process. As a result welding has only recently begun to realize the benefits of scientific research.

Semi-automated and automated, high deposition rate welding processes, such as Submerged Arc Welding (SAW), have been becoming more popular in order to reduce labor costs and increase productivity. The quality of a weld depends on the combination of base metal, filler metal, welding flux, and welding parameters used in producing the weld. In the SAW process the welding flux protects the weld metal from atmospheric contamination by burying the welding arc as well as forming a molten slag coating over the liquid weld metal.

The contamination of the weld metal with atmospheric oxygen and nitrogen greatly affects its mechanical properties, particularly fracture toughness. One of the main properties of a SAW flux is its ability, or lack of, to produce weld metal with a low oxygen content. Since SAW deposits have

low nitrogen levels, atmospheric oxygen is an unlikely source of contamination. The oxidation potential of a flux is commonly determined by the Basicity Index of the flux. The Basicity Index is an empirical formula, based on the chemical composition of the flux, by which the fluxes are rated as acidic, basic or neutral. In this context, the higher the Basicity Index the greater the basicity of the flux and the lower the oxygen content of the weld-metal. There is, however, little data on the actual oxygen availability in a given flux as a function of basicity.

The aim of this work is to determine by measurement the actual partial pressure of oxygen in molten SAW fluxes, which is commonly referred to as the oxygen pressure of the flux. The oxygen pressure is a measure of the attraction for oxygen by the molten flux, which is composed mainly of oxides. Any specific combination of oxides will have a unique oxygen potential which will depend only on the temperature and the pressure of the system. The oxygen pressure is a major factor in determining the extent of slag-metal reactions which occur during welding.

The development of oxygen concentration cells, especially the disposable oxygen probes, has provided a quick and easy method of determining the oxygen activity in liquid steel. Recent success with these probes in measuring the oxygen pressure in steelmaking slags (ref. 1,2) has led to the idea of using them to measure the oxygen pressure of molten SAW fluxes.

The oxygen pressure of fluxes and its variance with temperature will give an insight into the fluxes potential contribution to the oxygen content of the weld metal as well as assist scientists in determining the thermodynamics and kinetics of the chemical reactions occurring during welding.

B. THE SUBMERGED ARC WELDING PROCESS

In the SAW process the heat of fusion is supplied by an electric arc between a bare metal consumable electrode and the work piece. The electrode feed rate, welding current and the welding voltage are controlled by the welding machine in order to maintain a stable welding arc. In the constant current system the electrode feed rate is varied in order to maintain a constant voltage. The constant potential system allows the current to vary in order to maintain a constant electrode feed rate. The process is made either automatic or semi-automatic depending on whether the travel speed is automatically controlled or controlled by manual movement of the welding torch. The SAW process has been successfully used with very high travel speeds. The ability to use several electrodes in tandem has resulted in weld metal deposition rates in excess of 10 kg/h (ref. 3) as compared to approximately 1 kg/h achieved in shielded metal arc welding (i.e. stick welding).

The flux in the SAW process completely buries the welding arc. A typical setup has the flux deposited just before the arc and then the excess flux removed with a vacuum after the weld has been made, as shown in Figure 1. A balance must be achieved between the chemical, electrical and physical properties of the flux. The flux must have adequate electrical characteristics to be able to support the welding arc. The molten flux protects the weld pool from the atmosphere physically by forming a slag

layer over it. The physical properties of the flux, such as viscosity and density, also affect the appearance of the final weld bead. The flux creates slag-metal and gas-metal reactions which affect the weld metal's final composition. The fluxes often contain deoxidizers, such as aluminum or silicon, in order to reduce the final weld metal oxygen content. When welding alloy steels, ferro-alloys (e.g. FeCr or FeNi) may be added to the flux to produce the desired alloy content in the weld metal. This is often done instead of using an alloyed filler metal (ref. 3).

The typical weld metal produced with various types of fluxes is shown in Figure 2. Fluxes containing high amounts of SiO_2 and MnO, produce high weld metal oxygen content, restricting their use to when fracture toughness is not a critical design factor. The superior electrical properties of these fluxes stabilizes the welding arc, allowing faster welding speeds and higher heat inputs. Lower oxygen welds are typically produced by increasing the amounts of CaO, MgO or CaF_2 in the flux. In addition, replacing the SiO_2 with Al_2O_3 and/or TiO_2 aids in reducing the oxygen content but still maintain desirable physical properties in the flux. Such fluxes are harder to use in welding, requiring slower welding speeds and tighter control of welding parameters. Slag removal after welding is often harder, requiring chipping or grinding to remove all the slag. Thus productivity appears to

be the trade-off for high quality, high toughness welds. Greater knowledge of the properties of different fluxes and the effects of various constituents of the fluxes will lead to increased productivity and maintain high quality welds.

C. IMPORTANCE OF OXYGEN IN WELD METAL

The oxygen potential of the welding flux influences the loss or gain of alloying elements and the number, type, and size of oxide inclusions in the weld metal. The effects of the loss or gain of alloying elements on the mechanical properties of the weld metal will depend on the effects of the alloying element and the quantity in which it is present. Usually an optimum quantity of the various elements is desired. The composition of the flux must be matched with the proper base and filler metal to achieve the desired weld metal composition. For example, a high SiO_2 flux would probably be combined with a low Si electrode in order to prevent too high Si content in the final weld metal.

Oxygen is almost completely insoluble in solidified weld metal, thus it is present in the weld metal in the form of oxide inclusions. The effects of a high inclusion level in plain carbon and C-Mn steels is to provide an easy fracture path and many fracture initiation points. The variation of toughness with oxygen content of the weld metal was shown earlier in Figure 2. Superior toughness, especially upper shelf toughness, is achieved by reducing the number and size of inclusions present in the weld metal.

Recent work with microalloyed steels has shown that too low an oxygen content in the weld metal can also decrease the weld metal fracture toughness. It has been found that an acicular ferrite structure in the weld

metal is primarily responsible for high toughness (ref. 4). The random orientation of the fine grained (3 - 5 μm) structure of acicular ferrite provides maximum resistance to crack propagation. In order to maximize this structure in the weld metal the oxygen content must fall within a specific range, which will depend upon the composition of the weld metal and its cooling rate.

Acicular ferrite is formed from austenite grains at intermediate cooling rates between polygonal ferrite and upper bainite formation (Figure 3). Acicular ferrite is nucleated within the austenite grains by oxide inclusions. Grain boundary ferrite will tend to form along the austenite grain boundaries. Sideplate ferrite, an upper bainite type structure, grows from the grain boundary ferrite into the grain. With proper control over cooling rates and the addition of microalloys which suppress grain boundary ferrite formation, a weld metal microstructure of nearly 100% acicular ferrite can be achieved.

The effect of increasing the oxygen content (e.g. > 500 ppm) of the weld metal will shift the cooling curve (Figure 3) such that higher temperature transformation products will form. The precipitation of stable oxides will minimize grain growth increasing the grain boundary area and thus promoting grain boundary ferrite. The large number of oxide inclusions

provide energetically favorable nucleation sites for the formation of ferrite. Thus the microstructure will consist mainly of polygonal and grain boundary ferrite.

If the oxygen content is too low (e.g. < 200 ppm) the transformation at the austenite grain boundaries will be suppressed due to fewer nucleation sites. Fewer inclusions also suppresses acicular ferrite formation resulting in low temperature transformation products such as bainite or martensite to form within the austenite grains. This will substantially reduce the weld metal toughness and possible result in brittle failures. Although the level of oxygen inclusions required depends on the chemistry and cooling rates, it is clearly seen that control over the oxygen content is essential to predict the microstructure and toughness of microalloyed steels.

D. SOURCES OF OXYGEN

The four possible sources of oxygen in a SAW weld are the filler metal, base metal, atmosphere and the welding flux. The oxygen content in the filler and base metal is typically less than 100 ppm and may even be as low as 10 ppm. Their contribution to the weld metal can easily be determined from chemical analysis of the steel.

The extent of atmospheric contamination of the weld metal is not precisely known. For acidic and mildly basic fluxes the contribution of air to the oxygen content of the weld is not significant. With very basic fluxes, when a low oxygen content is desired, the atmospheric contamination may have greater significance (ref. 5,6). It is known that the nitrogen content of SAW welds is lower than with most other welding processes as shown in Figure 4. This suggests that the atmospheric contamination of SAW weld is low and thus the oxygen pickup from the atmosphere is also low.

For most SAW fluxes it is reasonable to conclude that the flux is the major contributor of oxygen to the weld metal. The nature of the methods of transfer of oxygen to the weld metal is an area of ongoing research. It is theorized the flux partially decomposes into suboxide and vapor in the electric arc. SiO_2 may form the suboxide SiO which is then dissolved at the electrode tip as [Si] and [O]. Similarly, highly volatile oxides such as MnO

will vaporize and dissolve in the metal droplets as [Mn] and [O] (ref. 7). It is known that gas-metal reactions occur at the electrode tip resulting in high oxygen levels in the molten droplets which are transferred to the weld pool (ref. 8).

The high oxygen content of the droplets adds more oxygen to the weld than there can be accounted for in the final weld, even when the base metal dilution is taken into consideration. Slag-metal reactions must occur in order to reduce the oxygen level to its final state. The high temperatures experienced in welding help to offset the short reaction times, thus allowing some reactions to occur. Reactions which are kinetically favored will approach equilibrium in the short reaction time. Slower reaction will not reach equilibrium and may not occur even though they are thermodynamically favored. Slag-metal reactions that are of importance include the deoxidation reactions of any Al, Ti or Si that may have been added to the flux as deoxidizers. Ferro-alloys that have been added to the flux when welding alloy steels must also travel from the flux to the weld metal.

Additional oxygen may result in the weld metal from slag entrapment. This source is likely to be minimized by the vigorous stirring in the weld pool caused by Lorentz forces. Lau et al. (ref. 8) found that flux entrapment was not a major source of oxygen. They concluded that the major source of

oxygen was from the decomposition of the flux and the major sites of oxygen absorption are the electrode tip and droplet stage. They also concluded that the final oxygen level in the weld metal was determined by deoxidation and the separation of these oxidation products to the slag.

CHAPTER II

A. STRUCTURE OF SILICATE MELTS

The majority of the welding fluxes used for SAW contain a large percentage of silica. The fundamental structure of silica is the SiO_4^{4-} tetrahedron which consists of highly covalent Si-O bonds. The small Si^{4+} cation is surrounded by four large O^{2-} anions, each of which is shared by the corners of neighboring tetrahedra. The crystalline structure of silica consists of a hexagonal lattice of Si^{4+} ions, each sharing four tetrahedrally arranged oxygen atoms, and extending symmetrically in three dimensions.

In the molten state the tetrahedra remain but the three dimensional network becomes less ordered (Figure 5) and dissociates into smaller complex anions. In order to minimize the charge, molten silica forms ring structures of large anions which have only a small negative charge. For example the anion, $Si_9O_{21}^{6-}$, has been proposed to result from the reaction (ref. 9)

$$21SiO_2 = 2Si_9O_{21}^{6-} + 3Si^{4+} \quad \text{.....(1)}$$

As the temperature of the melt increases the degree of dissociation increases, creating smaller anions and more cations. This is observed

physically by a decrease in the viscosity of molten silica as the temperature is raised.

Silicates are composed of two types of oxides. "Network formers" (such as SiO_2, Al_2O_3, P_2O_5 and TiO_2) are oxides which can polymerize to form interconnected three dimensional networks. Al^{3+} can replace Si^{4+} in a silicate melt at some times as will be discussed later. TiO_2 on the other hand forms a separate three dimensional structure when in solution with SiO_2 (ref. 10).

Most other metal oxides (MO) form a more ionic bond with oxygen and dissociate into simple ions.

$$MO = M^{2+} + O^{2-} \quad \text{.....(2)}$$

When these oxides are mixed with silica they supply extra O^{2-} ions to the silica network. This allows the silica network to dissociate without forming any Si^{4+} cations since the M^{2+} cations will balance out the charge. These oxides are referred to as "network modifiers" because of their dissociation effect on the silica network.

The degree of polymerization of a silicate is indicated by the non-bridging oxygen per silicon (NBO/Si). A non-bridging oxygen is one which terminates the silica network by only joining with one Si atom. Pure SiO_2 has a NBO/Si = 0 meaning that it is fully polymerized. As more network modifiers are added to the silicate the NBO/Si increases and the degree of polymerization decreases. At the orthosilicate composition, NBO/Si = 4, the structure can be thought of containing only discrete SiO^{4-} anions and M^{2+} cations. This is a simplification of the actual situation as will be discussed later (ref. 10).

B. BASICITY

The addition of a network modifier to a silicate melt can be represented by the following equation.

$$O^0 + O^{2-} = 2O^{1-} \quad \text{.....(3)}$$

We can define three distinct types of oxygen in the melt. Bridging oxygens, O^0, are the oxygen connecting two SiO_4^{4-} tetrahedra. The non-bridging or terminal oxygens, O^{1-}, are located at the ends of the network chains. Free oxygens, O^{2-}, are the extra oxygens from the network modifiers that are not associated with the silica network.

It is easy to imagine that as O^{2-} anions are added to the melt they are used up by the O^0 oxygens. At the orthosilicate composition (NBO/Si=4) all the O^0 oxygens are used up so that all the oxygen is present as O^{1-} anions. A basic slag can be defined as one that has a higher network modifier composition than the orthosilicate, resulting in the presence of free oxygen. An acid slag has no free oxygen ions and the more O^0 it contains the more acidic it is.

It is quite likely that at any composition the silicate will have some of each type of oxygen. The equilibrium constant for Equation 3 is

$$K = \frac{[O^{1-}]^2}{[O^0]*[O^{2-}]} \quad \text{.....(4)}$$

For any value of K other than infinity or zero there will always be some of each type of oxygen as shown in Figure 6. In order to better reflect the silicate structure, basicity is defined as the concentration of O^{2-} anions. A high concentration of O^{2-} indicates a high concentration of network modifiers thus making it basic. The lower the O^{2-} concentration the more acidic the silicate. Part of the confusion surrounding the term basicity stems from the fact that it is not possible to measure the concentration of O^{2-} anions. Most basicity determinations are based solely on empirical formulas relating the basicity to the composition of the melt.

Acid oxides are defined as "oxygen acceptors" which are the network formers. "Oxygen donors" are the basic oxide or the network modifiers. Some oxides, such as Al_2O_3, can behave either as an acid or a base. These amphoteric oxides behave as a base in an acidic slag and as an acid in a basic slag. In the case of Al_2O_3 the network forming capability depends on the network modifiers present. Al_2O_3 acts as a network former by Al replacing some of the Si atoms in the network. Al^{3+} is not able to replace a Si^{4+} in the network without picking up an extra positive charge from

another cation. Thus when there are not enough cations present, as in an acid slag, Al_2O_3 will merely dissociate into ions and act as a base. When the Al^{3+} does become part of the network the strength of the Al-O bond will be greatly influenced by the cation from which the Al^{3+} is receiving its positive charge. The effect of Al_2O_3 on a slag will not only depend on the amount of network modifiers but also on the type.

C. BASICITY RATIOS

As mentioned earlier, the activity of O^{2-} in a slag cannot be measured. In practice, the basicity of slags is expressed as ratios of its acid and basic components. The effectiveness of any one component in a slag as a base will depend on what other oxides are present. Any general empirical formula will only give an approximation or rough relation to the actual slag basicity.

One of the first basicity ratios was the ratio of the weight percent of the oxygen from the basic oxides to that of the silica. A list of this and several other basicity ratios is given in Table 1. Probably the most extensively used basicity ratio was the "V" ratio which is the ratio of the weight percent of CaO to SiO_2. It was used in the steel industry to estimate the sulphur and phosphorous capacity of the slag. Other ratios evolved from the "V" ratio in order to take into account other oxides present in the slag. Although the equations become quite complex, there is still no theoretical support for any one equation over the other.

The basicity ratios used in the welding field are different from those used in steelmaking. This is due to the very different conditions experienced in welding than in steelmaking. In welding the high temperatures and short reaction times mean that the various slag-metal reactions approach

equilibrium to different degrees. Also, the basicity ratios used in welding were developed to relate the flux composition to the weld metal oxygen content. There is no reason why flux basicity would affect its ability to give up oxygen to the weld metal.

The International Institute of Welding (IIW) uses the Basicity Index proposed by Tuliani et al. (ref. 11) in 1969.

$$BI\ (IIW) = \frac{CaO + MgO + BaO + SrO + Na_2O + K_2O + Li_2O + CaF_2 + 0.5(MnO + FeO)}{SiO_2 + 0.5(Al_2O_3 + TiO_2 + ZrO_2)} \quad \text{.....(5)}$$

The most unusual thing about this formula is the inclusion of non-oxide component, CaF_2. It has been argued that the CaF_2 has no effect on the basicity of a slag and that it should not be included (Ref. 6). Experimental data has shown that there is a better relationship between BI and the weld metal oxygen content if the CaF_2 term is included (ref. 4) (Figure 7).

D. OPTICAL BASICITY

The ionic nature of any chemical bond is determined by the affinity for electrons of the two species of the bond. Oxygen has a relatively high affinity for electrons. Thus, when bonded to other elements with a high electron affinity, such as Si, they will form a highly covalent bond. If the other element has a low affinity for electrons then the bond will be strongly ionic. The oxygen atoms become polarized when they form a covalent bond with a cation. The greater the covalent nature of the bond the greater the polarization. In an oxide, the polarization of the oxygen ion determines the residual negative charge on the oxygen ion and thus its electron donor power.

A recent introduction to the analysis on the chemical properties of metallurgical slags is the concept of Optical Basicity, which is based on principles of Lewis basicity (ref. 12,13,14). Basicity is related to the electron donor power of the oxygen in the slag. This is determined by the average residual negative charge of the oxygen after it has satisfied the bonding requirements of neighboring cations. An acid slag will have a high percentage of covalent bonds resulting in a low average negative charge on

the oxygen ions. A basic slag will be just the reverse. The optical basicity is thus determined by the effect of the cations on the oxygen ions present in the slag.

The optical basicity is determined by introducing a trace amount of a probe ion, such as Pb^{2+}, into the slag. The negative charge donated to the probe cation by the oxygen anion is a measure of the electron donor power of the oxygen. The electron donation to the probe ion results in an expansion in the "s" and "p" orbitals of the ion and is related to the nephelauxetic effect (ref. 13). This reduces the energy in the ultraviolet absorption band of Pb^{2+} ions in the slag compared with free (gaseous) Pb^{2+} ions. This can be observed spectroscopically, hence the term "Optical" basicity, as a "red" shift in the spectrum of Pb^{2+} ions. A value of optical basicity of unity has been given to pure CaO such that all measurements for other oxides and slags will be related to this base.

Pauling's Electronegativity is a measurement of the affinity of an atom for its valency electrons. A direct relationship has been found between the Optical Basicity as measured with spectroscopic techniques and the Pauling's Electronegativity of the cations in the slags. The basicity of a slag can be calculated from the sum of the optical basicities of the component oxides multiplied by their equivalent cation fraction.

$$B = B1*X1 + B2*X2 + B3*X3 + B4*X4 \quad (6)$$

The equivalent cation fraction, X, is the fraction of negative charge which is balanced by the positive charge (i.e. oxidation number) of the cation. The optical basicity of each oxide can be calculated from Pauling's Electronegativity by the relationship

$$B = [1.36(x - 0.26)]^{-1} \quad (7)$$

where x is the Pauling's Electronegativity. Thus basicity can be calculated directly from a chemical analysis of a slag. This makes possible the determination of basicity of slags which are opaque in the UV region or where experimental determination would otherwise be difficult.

Although initial success with this method is promising, the relationship is not exact and some discrepancies have been found. In particular the above relationship does not apply to the transition metals. The measurement of optical basicity of slags with transition metals may also be affected by the presence of other ions and metallic bonding (ref. 14).

E. OXYGEN POTENTIAL

The oxygen chemical potential is the change in Gibbs free energy of oxygen from its standard state (1 atm pressure) to its present state. This can be easily calculated from the measurement of the oxygen pressure for any system.

$$\Delta G^{\circ} = RT \ln pO_2 \quad \text{.....(8)}$$

where R is the molar gas constant, T is absolute temperature, and pO_2 is the partial pressure of oxygen.

The oxygen potential can be used to measure the stability of an oxide. The free energy of formation of an oxide is the energy associated with the formation of an oxide from its elements. For example the free energy of formation of MnO is

$$2Mn + O_2 = 2MnO \qquad \Delta G^{\circ} = -798500 + 164T \text{ J/mol } O_2 \quad \text{.....(9)}$$

at standard conditions (ref. 15). When the oxide and metal are in their pure states the equilibrium constant for Equation 9 is

$$K = 1/(pO_2) \quad \text{.....(10)}$$

therefore

$$\Delta G^\circ = -RT \ln(1/pO_2) \text{ or } \Delta G^\circ = RT \ln(pO_2) \quad \text{.....(11)}$$

The oxygen potential becomes equal to the free energy of formation of the oxide. Stable oxides have high negative free energies of formation, and are less likely to be involved in any chemical reactions.

Slags are composed mainly of a mixture of oxides. The equilibrium of any chemical reaction will depend on the "active mass" of the oxide taking part. For ideal solutions the active mass is the molar fraction of the oxide. Most solutions are not ideal, therefore the term "activity" is used to represent the actual active mass. A pure oxide will have an activity of unity whereas an oxide in a mixture will have an activity less than unity.

The activity is a measure of the attraction of the rest of the slag for an oxide. If there is a great attraction then the activity will be lower than the actual molar fraction of that oxide. This means that the effective concentration is lower than the real concentration and thus any chemical reactions will be inhibited. The activities of oxides in a slag indicate the extent to which they will react with a metal. This is used in steelmaking to

determine the amount of sulphur, phosphorous, oxygen, alloying elements, etc. which will be in the steel and the slag when equilibrium is reached.

The oxygen potential of the oxides in a slag will depend on their activities. As the activity of an oxide becomes increasingly lower its oxygen potential becomes more negative. Take for example Equation 9 where MnO is in a slag. The oxygen potential becomes

$$\Delta G = \Delta G^{\circ} + RT \ln(a(MnO)/pO_2) \quad \text{.....(12)}$$

where ΔG° is the standard free energy of formation given in Equation 9, ΔG is the actual free energy of formation and a(MnO) is the activity of MnO in the slag. From this it is seen that if the a(MnO) is lowered the ΔG for Equation 9 becomes more negative. The relative stability of various oxides will depend to a certain extent on the slag composition by its effects on the activities of the oxides.

F. ESTIMATION OF WELD METAL OXYGEN

It is not practical to attempt to predict the exact weld metal oxygen content of any one weld due to the large number of variables which affect it. Factors such as dirt, moisture or segregation within the metal or flux are just a few of the things which may have an effect. Fluxes can be rated according to which one is more likely to result in higher weld metal oxygen than another, or to predict in what range the oxygen content of the weld metal will be with a particular flux.

The most common property used to rate fluxes according to their potential to give oxygen to the weld metal is basicity. Although basicity has no direct relationship to the oxygen potential of a flux, the most common basic oxides tend to be very stable oxides and the most common acid oxides tend to be relatively weak.

The basicity index most widely used in industry is the IIW basicity index given earlier as Equation 5 and is the one referred to hereafter as "BI". The relationship between oxygen content and the BI is shown in Figure 7. The weld metal oxygen rapidly increases when the BI drops below 1, which indicates an acid flux. Neutral fluxes have a BI between 1 and 1.5 and basic fluxes have a BI >1.5. It is seen from Figure 7 that the oxygen content reaches a minimum of about 200 ppm. Lower oxygen content may

be reached by adding deoxidizers to the flux but not by lowering the basicity. The large amount of scatter in Figure 7 shows that the BI is a not an accurate indicator of weld metal oxygen.

The oxygen potential of the oxides is used to some extent in predicting the weld metal oxygen content. Fluxes claiming to produce low oxygen welds often contain only fairly stable oxides (i.e. low oxygen potential) with very few weak oxides such as MnO and FeO. Low oxygen welds can be produced with fluxes which contain low amounts of SiO_2, MnO and FeO. In their standard state the most common oxides in SAW fluxes at 1600 °C are given the following order of stability: CaO, Al_2O_3, MgO, TiO_2, SiO_2, MnO and FeO. In a study done by Chia and Eagar (ref. 16) using binary fluxes containing CaF_2 and a metal oxide, where CaF_2 was considered inert, the stabilities of the above oxides were given the following slightly different order: CaO, TiO_2, Al_2O_3, MgO, SiO_2 and MnO. FeO was omitted from the study because of its low content in many SAW fluxes. This is probably a better indicator since it was done at welding temperatures with molten oxides. This study ignored any possible interactions between CaF_2 and the various metal oxides. In many cases CaF_2 and an oxide form two immiscible liquids, such as in the CaF_2-SiO_2 phase diagram. This increses the oxide activity in the binary melt. CaF_2 and SiO_2 may also react chemically to form SiF_4(g), $CaSiO_3$ and CaO (ref. 19).

It is claimed by some that the use of basicity ratios to reduce the weld metal oxygen is incorrect (ref. 17). It is known that a low basicity or high oxygen potential results in high oxygen welds. This is partly due to the fact that SiO_2, the most extensively used acid oxide, has a relatively high oxygen potential. CaO has been traditionally used in great amounts in basic fluxes and is also a highly stable oxide. Thus the correlation between oxygen potential, basicity and weld metal oxygen has more to do with the historical development of fluxes than with any real relationship. In fact it is known that fluxes high in FeO and MnO, weak basic oxides, will produce high oxygen welds. Recently developed fluxes based on TiO_2 rather than SiO_2 are claimed to produce low oxygen welds with acidic fluxes. This is due to the higher thermodynamic stability of TiO_2.

The weld metal oxygen has been estimated from equilibrium data and concentration of specific oxides present in the slag. In particular Eagar (ref. 6) has suggested that the activities of SiO_2 and/or FeO should be correlated with the weld metal oxygen content. Eagar has proposed the weld metal oxygen of acid and slightly basic (BI < 2) fluxes is dependent on the reaction of SiO_2.

$$SiO_2 = [Si] + 2[O] \quad \text{.....(13)}$$

The calculated equilibrium weld metal oxygen for $CaO-SiO_2$ slags of varying CaO/SiO_2 ratios at 2000 °C is shown in Figure 8. For basic fluxes (BI > 2) he proposed that the oxygen content was limited by the FeO reaction.

$$Fe + [O] = FeO \quad \text{.....(14)}$$

This would prevent the weld metal oxygen from dropping to base metal levels no matter how high the basicity. Although it is unlikely that this reaction will reach equilibrium during welding, it will provide oxygen to the weld metal in attempt to reach equilibrium. Figure 8 also shows the theoretical equilibrium weld metal oxygen content for basic slags using $CaO-SiO_2$-FeO slags of varying CaO/SiO_2 ratios.

G. OXYGEN PRESSURE OF SLAGS

The oxygen pressure of a slag is dependent on the oxygen potential of the oxides present in the slag. It is a measure of the slag's overall attraction for oxygen. A low oxygen pressure indicates that the slag is very stable and will not readily give up oxygen. A high oxygen pressure indicates that the slag will readily give up oxygen.

The oxygen pressure of a slag can be brought into equilibrium with the atmosphere it is melted in. The rate of this reaction will depend on the diffusivity of oxygen in the slag and the oxygen gradient between the atmosphere and the slag. The oxygen pressure is still a measure of the slag's attraction for oxygen. The composition is changed by the fact there is more oxygen in the slag. This is more readily seen in slags which contain an oxide which can change valence states. The extra oxygen promotes the higher valence state until the equilibrium ratio between the valence states is reached for the oxygen pressure of the atmosphere.

The oxygen pressure in a slag is extremely important in determining the thermodynamics of slag-metal reactions. The oxygen pressure does not necessarily promote the same reactions as the basicity of the slag. A good example is the two processes of desulphurization and dephosphorization of

steel during steelmaking. The desulphurization reaction is represented as

$$\%\underline{S} + O^{2-} = S^{2-} + \%\underline{O} \quad \text{.....(15)}$$

A high basicity and a low oxygen pressure will aid in removing sulphur from the steel. These conditions are also conducive to producing low oxygen welds as mentioned earlier. The dephosphorization reaction can be represented as

$$2\%\underline{P} + 5\%\underline{O} + 3O^{2-} = 2PO_4^{3-} \quad \text{.....(16)}$$

The removal of phosphorus from steel is facilitated by high basicity and high oxygen pressure (ref. 18).

The oxygen pressure of a slag varies not only with slag composition but also with temperature. The increase in oxygen pressure may be important in determining the extent of reactions at high temperatures. This is especially important in welding where extensive thermodynamic data at welding temperatures is not available. The increase in oxygen pressure of the flux with temperature will indicate how the oxygen potential of the flux increases with temperature. This extra knowledge can be used with the increase in reaction times to predict the extent of the various possible slag-metal reactions.

CHAPTER III

A. IONIC CONDUCTION

The oxygen concentration cells used to measure oxygen pressure in metal, mattes and slags are based on oxygen ion conductors. Ionic conductors allow only one ionic species to be transmitted through them, in this case oxygen anions. They also act as insulators to electrons and electron holes. Oxygen ionic conductors are oxides which conduct oxygen ions only within a certain temperature and pressure range, therefore the choice of conductor will depend on its application.

In any material there are four possible carriers of current: electrons, electron holes, anions and cations. Electrons are very small thus have a very high mobility when free. Electron movement is restricted when they are tightly bound to an atom, requiring a large amount of energy in order to free them. An electron hole has the opposite charge to an electron. It occurs when an electron is vacant from an atom, leaving an extra positive charge. A neighboring electron fills in the hole, effectively moving the hole by one position. This continues such that the hole is moved in the direction of current flow.

The mobility of ions is much less than electrons due to their larger size. In an ionic conductor the conduction of electrons and electron holes must be minimized and the conduction of ions greatly facilitated.

Ionic conduction is made possible by the presence of point defects in the crystal lattice. All materials have some point defects but it is the concentration and mobility of the particular defects which will determine the materials ionic conduction properties. The several types of defects which are possible in an ionic crystal MX are listed below using the Kroger-Vink notation (ref. 20). (In the Kroger-Vink notation the superscript "O" denotes an effective positive charge and "'" an effective negative charge. The subscripts denote the location of the ions (M and X) or the vacancies (V).)

a) Vacancies: These occur when there is a missing M^+ or X^- ion. They create the vacancies V_M' or V_X^O respectively.

b) Interstitial atoms: Either M^+ or X^- may occupy an interstitial site in the crystal lattice. This creates the defects M_i^O and X_i' respectively.

c) Misplaced atoms: One species may occupy the normal site of the other species giving the possible defects M_X and X_M.

d) Schottky defects: When both a cation and a anion are vacant from their lattice site it is referred to as a Schottky defect (V_M', V_X^O).

c) Frenkel defect: This occurs when a cation moves to an interstitial site leaving a cation vacancy (V_M') and an interstitial catien (M_i°). This may also happen to anions creating the defects V_X° and X_i'.

The introduction of impurity ions into an ionic crystal lattice creates a large number of defects. They may enter as interstitial ions or they may replace ions on the lattice (substitutional). If the ion has the same valence as the original ion for which it is substituted, there will be no charge effect caused by the defect. If the valency is different, as is often the case, then the charge may be balanced with either a vacancy or an interstitial ion. Many types of defects may coexist in an ionic crystal. Energy considerations usually favor one type of defect under a set of conditions of temperature, pressure, crystal structure and impurity type.

B. OXYGEN CONCENTRATION CELLS

An oxygen concentration cell consists of a solid oxide electrolyte (oxygen ion conductor) separating two compartments of different oxygen partial pressure (Figure 9). The difference in oxygen pressure creates a potential for oxygen ion transfer from one side to the other through the solid electrolyte. If the electrolyte is a pure ionic conductor then no oxygen can be transferred without an external electrical connection to complete the electrical circuit.

The net reaction for transferring oxygen from the high oxygen pressure side to the low oxygen pressure side of the electrolyte is

$$O_2\,(pO_2(1)) = O_2\,(pO_2(2)) \quad \text{.....(17)}$$

The energy change for this reaction is

$$\Delta G = -RT \ln (pO_2(2) / pO_2(1)) \quad \text{.....(18)}$$

Since $\Delta G = -nFE$ where E is electrical potential and "F" is Faraday's constant then Equation 18 can be expressed as

$$E = (RT/4F)\ \ln(pO_2(2)/pO_2(1)) \quad \text{.....(19)}$$

If the oxygen pressure on one side of the solid electrolyte is known than the oxygen pressure on the other side can be calculated from Equation 19 by measuring the electrical potential of the cell (Figure 9).

The most commonly used solid electrolyte used in high temperature metallurgy is ZrO_2 doped with CaO. The Ca^{2+} ion occupies a Zr^{4+} site causing a oxygen vacancy to balance the charge.

$$(CaO) = Ca_{Zr}'' + V_O^{oo} + ZrO_2 \quad \text{.....(20)}$$

For each mole of CaO dissolved in ZrO_2 there is one mole of oxygen vacancies created. Thus the electrolyte contains a high concentration of only one type of ionic defect. O^{2-} ions move from one vacancy to the next creating a current flow through the electrolyte. If the electronic conduction is low enough then the material will be considered a pure ionic conductor. The ionic conduction increases with increasing dopant content due to increasing ionic defects. At higher concentrations, from 3% to 4% depending on the electrolyte, the defects become ordered and the ionic

conductivity decreases. In many cases a higher concentration of a dopant leads to the formation of a new compound. Figure 10 shows the ionic conductivity for several common electrolytes with increasing dopant content.

C. ELECTRONIC CONDUCTION

Most solid electrolytes are pure oxygen ionic conductors only over a certain temperature and pressure range. The total conductivity must be more than 99% ionic in order to be considered a pure ionic conductor. Electronic conduction becomes substantial at both low and high pO_2. At low pO_2 oxygen is removed from the lattice of the electrolyte creating free electrons (n-type semiconduction).

$$O^{0} = V_O^{oo} + 2e' + 1/2O_2 \quad \text{.....(21)}$$

When the pO_2 is high excess oxygen is accommodated into the electrolyte lattice creating electron holes (p-type semiconduction). The oxygen may enter as interstitial atoms or create a cation vacancy in the lattice.

$$1/2O_2 = O_i'' + 2e^{\circ} \quad \text{.....(22)}$$

$$\text{or} \quad 1/2O_2 = V_M'' + 2e^{\circ} + MO \quad \text{.....(23)}$$

The useful range of pO_2 of an electrolyte will depend on the temperature, the electrolyte and the impurity content of the electrolyte material.

In order to increase the useful range of an electrolyte an approximation of the contribution of electronic conduction to the total conduction of an electrolyte can be calculated for small amounts of electronic conduction. The cell EMF for an oxygen concentration cell used in low pO_2 is

$$E = (RT/F) \ln((pO_2(2)^{1/4}+p\Theta^{1/4}) / (pO_2(1)^{1/4}+p\Theta^{1/4})) \quad (24)$$

from which an unknown pO_2 can be calculated (ref. 21). In the above equation $p\Theta$ is the oxygen partial pressure at which the ionic conductivity is equal to the electronic conductivity. The value of $p\Theta$ depends on the specific electrolyte used. It has been determined for many commercially available solid electrolytes (ref. 21,22,23). $p\Theta$ depends to some extent on the level of unwanted impurities in the electrolyte and on the processing of the electrolyte.

D. DISPOSABLE OXYGEN CONCENTRATION CELLS

In the metallurgical field, the oxygen concentration cells are immersed into liquid metal, matte or slag to determine the oxygen partial pressure of the melt. These cells are often referred to as oxygen probes or sensors. The most common use is in measuring the oxygen content of liquid steel. The attack of liquid steel and steelmaking slags on the oxygen probes has led to the development of disposable probes, oxygen concentration cells used for just one reading. The attack of the melt on the electrolyte does not influence its effectiveness but limits its life.

There are three basic designs of disposable oxygen probes, shown in Figure 11, referred to as the plug, tube and needle type probes. The tube types consist of a thin walled tube of the electrolyte material containing the reference material and an electrical contact. The tube cells are the most common due to the development of high density, doped zirconia tubes that can withstand the thermal shock of being immersed directly into molten steel. The response time for the EMF readings of the cell to stabilize is very fast due to the thin tube walls. The external electrode is attached simply by winding it around the outside of the tube. The simplicity of construction and good results with this probe design make it very popular.

The plug type oxygen probe consist of a plug of electrolyte material in the end of a silica or alumina tube. The reference material is located inside the tube in contact with the electrolyte plug. The electrical leads must be attached to the plug both on the inside and outside of the tube. The plug type has the advantage of being more resistant to thermal cracking because the electrolyte is a flat disc and tends to be thicker. These probes take longer to stabilize but also last longer before being penetrated by the melt. It is often difficult to maintain a tight seal between the electrolyte and the tube during the thermal cycle it is exposed to. Alumina and silica tubes are less corrosion resistant to steelmaking slags than most of the electrolyte materials used. This is of greatest significance in laboratory experiments where the dissolved silica or alumina may alter the composition of the melt.

The needle probe was introduced in 1978 by Janke (ref. 24) as a cheaper oxygen probe for measuring the oxygen pressure of liquid steel. It consisted of a Mo wire that was thermally sprayed with a reference material (e.g. Cr/Cr_2O_3). This was then coated with a thin layer of the electrolyte by thermal spraying. He found their performance as good as commercially available tube type probes with which he compared them. Even at low oxygen pressure they gave readings similar to the tube probes. The fact that the electrolyte was less dense than the tube probes did not affect their

operation as long as it prevented the melt and the reference material from making contact. Needle probes have the advantage of being simple and cheap to manufacture and their response time is shorter due to the thin electrolyte coating.

Oxygen probes consist of a solid electrolyte, reference material and electrical leads. Therefore the two main factors which contribute to the cell performance are the choice of a solid electrolyte and reference material. The reference may be either a gas of fixed oxygen partial pressure or a solid oxide reference in equilibrium with its metal. The use of gas references allows for the easy adjustment of the oxygen pressure. Air is often used since it is cheap and does not require accurate mixing devices to control the oxygen pressure. Pure oxygen is also used in order to produce a reliable reference. Although gases may be mixed, such as Ar and O_2, to give any desirable oxygen pressure the attachment of accurate mixing devices makes the probes more cumbersome and the reference less reliable. Diffusion of gaseous oxygen through the electrolyte can occur, especially with electrolyte materials which are not fully dense. This creates an artificially high oxygen pressure reading in the melt. It is more substantial when using high oxygen partial pressure references such as air or pure O_2

due to the higher oxygen gradient across the electrolyte. It is also more difficult to securely attach the electrical leads to the electrolyte inside the probe when using a gas reference. It is suggested by some that gas references be only used for rigorously stirred steel melts with >150 ppm oxygen (ref. 25).

Solid references contain a mixture of a metal and its oxide. The oxygen partial pressure depends on the equilibrium of the metal-metal oxide reaction at a specific temperature. The oxygen pressure is not variable by the user but will change with temperature. If a different reference oxygen pressure is desired a different reference material must be used. It is important that the reference does not react with the electrolyte or the melt or have more than one possible equilibrium reaction. The most commonly used reference is Cr_2O_3/Cr which is used mainly for liquid steel. The equilibrium oxygen pressure of the reaction

$$2Cr_2O_3 = 4Cr + 3O_2 \quad \text{.....(25)}$$

is close to the oxygen pressure for deoxidized steel, making the EMF readings more reliable. The oxygen pressure is also at the limit for ionic conduction for most ZrO_2-based electrolytes, possibly causing some n-type

electronic conduction. The use of MoO_2/Mo reference has the advantage of being well within the ionic range of ZrO_2-based solid electrolytes (ref. 2). It has a higher oxygen pressure than the Cr_2O_3/Cr reference, thus is useful for measuring oxygen pressures closer to its range.

The polarization of the melt and the reference will have an effect on the accuracy of the determined oxygen pressure. If there is any electronic conduction, current will flow in the cell causing a buildup of oxygen anions on one side of the cell. This is more severe when the cell EMF is high, creating a large driving force for current flow. A high oxygen potential gradient may also cause transport of oxygen through the electrolyte. This is more significant with the use of O_2 or air references where the oxygen pressure is very high compared to the melt. This error can be minimized by using a reference with an oxygen pressure close to that of the melt it is measuring and by stirring the melt.

E. SOME APPLICATIONS OF OXYGEN PROBES

The use of oxygen probes in metallurgy is quite varied and expanding. The most extensive use of the probes is to measure the oxygen content of a liquid metal. In Japan alone 185000 oxygen probes were used in 1980 in steelmaking (ref. 26). The probes are used mainly for control over the deoxidation of the steel. The oxygen activity in the molten steel is related to the probe EMF by the equation

$$E = (RT/2F)\ln(a(O) / (pO_2(ref)^{1/2})) \quad (26)$$

Almost instantaneous oxygen contents of liquid steel are determined from the probes rather than having to do a chemical analysis. This allows the steelmaker to accurately and quickly determine the proper amount of deoxidizers (e.g. Al, Si) which he must add to the steel to obtain the desired oxygen content.

Oxygen probes are used in the glass industry to determine the oxidation state of molten glass. The oxidation state of the glass is important in the melting, refining and color determination of the glass. It is determined by the ratio of the different valency states of a polyvalent oxide, for example the Fe^{2+}/Fe^{3+} ratio for glasses containing iron. The oxygen pressure and

basicity of the glass as well as the type and concentration of polyvalent oxide present govern its oxidation state. If the basicity and the polyvalent oxide content are constant then the oxidation state can be monitored by monitoring the oxygen pressure of the glass.

Some research has been done in relating the basicity, oxygen pressure, temperature and oxidation state of a glass. Tran and Brungs (ref. 27) have found a good relationship between oxidation state, temperature and oxygen pressure for a disodium silicate glass containing less than 2% total Fe.

$$\log(Fe^{2+}/Fe^{3+}) = a + b(1/T) + c\log pO_2 \quad \text{.....(27)}$$

The coefficients a, b and c for this glass are given in Table 2. Goldman (ref. 28) found that the slope of $\log(Fe^{2+}/Fe^{3+})$ vs. $\log pO_2$ depends on the temperature and glass composition instead of being constant as suggested by Equation 27. He came up with a relationship between oxidation state and basicity for a constant temperature and oxygen pressure (Figure 12). A new measure of slag basicity has been proposed based upon the relationship with the oxidation state of the melt (ref. 1). The ratio of Fe^{2+}/Fe^{3+} is used as

the basicity indicator for different slags at the same temperature and oxygen pressure. Oxygen pressures can be controlled by equilibrating the slag with the furnace atmosphere.

The activities of oxides can be determined with the use of oxygen probes in complex oxide melts. One of the first applications was the determination of a(PbO) in PbO-SiO_2 melts. The oxide was melted in the presence of metallic Pb in order to establish an equilibrium between (PbO) and pure Pb. The a(PbO) was calculated from the cell EMF by the equation

$$EMF = E^\circ + (RT/2F) \ln(a(PbO)) \quad \text{.....(28)}$$

where E° is the cell voltage with pure liquid PbO at the same temperature.

The a(FeO) can be determined in steelmaking slags in a similar manner. Artificial and real slags were melted in ARMCO-iron crucibles so that equilibrium between the slag and the iron crucible would be established (ref. 29). The activity was determined from the Equation 28 (using FeO instead of PbO). In order to facilitate the Fe-FeO equilibrium, silver can be melted with the slag (ref. 2). Equilibrium is quickly established between the silver and the slag because it is a liquid-liquid reaction. The a(FeO) is determined as mentioned.

The oxygen pressure of steelmaking slags is important in controlling the dephosphorization and desulphurization of liquid steel as shown earlier by Equations 15 and 16. In situ measurement of the oxygen pressure would allow control over these processes rather than relying entirely on equilibrium thermodynamics. The oxygen pressure determined at any one time will indicate to the steelmaker what additions need to be added to the slag in order to optimize its usefulness. Better control over the reducing and oxidizing periods of the slag in electric arc furnace practice would also result from in situ measurements of the oxygen pressure. Oxygen probes have proven successful in both laboratory and LD converter slags (ref. 1).

CHAPTER IV

A. PROBE DESIGN

The oxygen probe used in this study was based on the needle probe developed by Janke (ref. 24). The modified probe design used in this study is shown schematically in Figure 13. A 1.5 mm diameter molybdenum wire was cut into 40 cm lengths. One end of the wire was cleaned by sandblasting and then oxidized in an oxygen-acetylene torch flame. Approximately 5 cm of the oxidized Mo wire was plasma sprayed with yttria doped zirconia. The parameters used in plasma spraying are given in Table 3. A 0.5 mm thick layer of $ZrO_2(Y_2O_3)$ was achieved with 10 to 15 passes of the spray torch.

The reference material in this probe design is the Mo wire. Oxidizing the outside of the wire ensures that there is some MoO_2 present in order to maintain an equilibrium between the Mo and MoO_2, and a stable and accurate reference oxygen pressure. The probe used in this study is simpler than that used by Janke because it does not have a coating of Cr sprayed over the Mo wire. A Cr/Cr_2O_3 reference material is desirable for steelmaking because its equilibrium oxygen pressure is close to the oxygen pressures experienced in deoxidized steel. Oxides have higher oxygen pressure and fluxes have a broad range due to the use of both acidic and

basic fluxes. For this reason, a reference material with a higher oxygen pressure is desired. The Mo/MoO_2 reference was chosen because it has been successfully used by others (ref. 2) at high temperatures. The Mo wire is also able to withstand the elevated temperatures experienced in the experiment and still provide the mechanical support for the probe.

The other electrode of the oxygen probe was made with a 6%Rh-Pt (Pt6Rh) thermocouple wire. The wire was wrapped around the end of the probe several times to ensure good connection. It was encased in a high purity alumina tube to prevent contact with the Mo wire, which would short circuit. The Mo and Pt6Rh wire were connected to a pure copper connector just outside the furnace. A slight error results from slightly varying temperatures at the Mo/Pt6Rh connection, but this was only in the order of 0.5 mV. Copper wire was used to connect the probe electrodes to a strip chart recorder to record the cell EMF.

B. FURNACE DESIGN

The furnace used in this study was built at the University of Alberta in the Welding Engineering Laboratory. A schematic diagram of the furnace is shown in Figure 14. The furnace was heated with $MoSi_2$ heating elements which surround a vertical 5 cm diameter alumina tube running through the center of the furnace. The top and bottom of the furnace was water cooled. The top contained two 5 mm holes directly above the crucible in order to insert the oxygen probe and a thermocouple directly into the melt. A third hole in the top was used as a gas inlet in order to control the furnace atmosphere. The exhaust gas was directed through a tube at the bottom of the furnace and into a ventilation system. The bottom of the furnace lowered out to allow the charge of the flux into a crucible. The crucible platform was lowered and raised by a motor with a variable speed control.

The furnace temperature was monitored with a B-type thermocouple located just inside the center of the furnace chamber. Temperature was controlled by a Eurotherm temperature controller and thyristor. Current flow to the elements was controlled manually by a 10 ohm variable resistor. The furnace remained on between experiments at 800 °C and could be increased to 1600 °C within 1 hour.

C. EXPERIMENTAL PROCEDURE

In a typical experimental run the furnace was set to the desired temperature and allowed to stabilize. A 5 cm high zirconia grain stabilized (ZGS) platinum crucible was charged about 3/4 full with a flux. The crucible platform was lowered out of the furnace, the crucible placed on the platform and then raised back into the furnace. Only platinum tipped tongs were used to handle the crucible to prevent contamination. The flux was left about 30 minutes to reach the furnace temperature and to establish equilibrium between its oxides. Industrial grade argon was purged through the furnace at a flow rate of 20 cm^3/s. This was done to minimize oxygen pick-up by the fluxes from the furnace atmosphere.

The oxygen probe was slowly lowered into the furnace's hot zone (i.e. to approximately 1 cm above the crucible) and held for approximately 5 minutes to reach the same temperature as the furnace. A Pt6Rh/Pt30Rh thermocouple was inserted into the molten flux to determine its actual temperature. The thermocouple EMF was read from a digital multimeter. The thermocouple was then removed from the melt to minimize contamination of the flux with the alumina sheathing of the thermocouple. The oxygen probe was then inserted into the melt and the EMF recorded on

a strip chart recorder. After several minutes, when either the probe readings remained stable or the EMF began to deteriorate, the probe was removed. The furnace temperature was then reset and allowed time to stabilize. The above procedure was repeated with a new probe at the new temperature.

When a different flux was used the old flux had to be removed from the platinum crucible. Most of the flux was removed by pouring it into a ceramic crucible immediately after removing it from the furnace. The remaining flux was removed by melting it with lithium metaborate ($LiBO_3$) at 1200 °C. The molten $LiBO_3$ dissolved the remaining flux and was then poured out of the crucible. The $LiBO_3$ remaining in the crucible was removed by dissolving it in boiling concentrated nitric acid.

CHAPTER V

A. $ZrO_2(CaO)$ VS. $ZrO_2(Y_2O_3)$ SOLID ELECTROLYTE

The initial probes were made with a 5%wt CaO-ZrO_2 solid electrolyte whose composition is given in Table 4. This electrolyte is the most common electrolyte used in industrial steelmaking for measuring the oxygen pressure of liquid steel. It has also been successfully used in oxygen sensors for steelmaking slags. It has shown good thermal shock and fair corrosion resistance. Slag attack on the probe does not affect its stability unless it penetrates more than two thirds of the electrolyte thickness (ref. 1). The electrolyte has been found to be an ionic conductor at oxygen pressures as low as 10^{-20} atm at 1600 °C (ref. 30). Values for $p\Theta$ are available from technical literature, thus the contribution of electronic conduction at low oxygen pressure can be readily calculated from Equation 24 given earlier.

Initial experimentation with this probe was done at 1643K with flux #20, an acidic flux whose composition is given in Table 5. The attack of the slag on the electrolyte was significant and prevented the cell EMF from

stabilizing for very long before the probe failed. The probe after the run was blackened and extensively cracked. Examination of a cross section of the probe (Figure 15) showed that the slag penetrated the probe to contact the Mo wire.

For comparison a Y_2O_3-doped ZrO_2 solid electrolyte was tried (see composition in Table 4). This electrolyte material has not been used as extensively as ZrO_2(CaO) and thus there is not as much data on its performance. CaO- or MgO-doped ZrO_2 is usually used whenever possible because of their cheaper cost and proven reliability. Y_2O_3-doped electrolytes are expected to have higher corrosion resistance than CaO- or MgO-doped ZrO_2. A 8%wt Y_2O_3-ZrO_2 oxygen probe was used in measuring the oxygen pressure in a sodium disilicate glass (ref. 31). The electrolyte showed superior corrosion resistance over a 5%wt CaO-ZrO_2 electrolyte. In previous work on molten SAW fluxes with ZrO_2(MgO) electrolyte (ref. 32) the author had been unable to obtain a stable EMF. The $p\Theta$ for $ZrO_2(Y_2O_3)$ has been published for temperatures up to 1700 °C (ref. 33) allowing the determination of electronic contribution to the total conduction of the electrolyte using Equation 24.

Initial use of the 8%wt Y_2O_3-ZrO_2 oxygen probe on flux #20 was successful. Although the EMF was not more stable than with the ZrO_2(CaO) probes the probes did not show any signs of attack by the flux. Examination of the

cross section of the probe (Figure 16) did not show any penetration of the electrolyte by the slag. Most of the cracks in the used electrolytes (Figure 16) occurred after they were removed from the slag while they were cooling down. This is proven by the fact that the cracks extend from the electrolyte through the slag coating, thus they must have occurred after the slag had solidified. The cracks probably initiated due to thermal strain in the thin brittle layer of slag, which coated the probe. The cracks then propagated through the electrolyte.

B. RESULTS

The oxygen pressures of six different fluxes were examined in this study. The composition of the fluxes is given in Table 5. Fluxes #1, #3 and #4 were specially made from reagent grade oxides to form flux compositions similar to commercial fluxes. Fluxes #20, #50 and #91 are commercial fluxes. The oxygen pressure of flux #4 could not be determined because of its rapid penetration of the probes.

A 2-3 kg sample of each flux was used. The chemistries of the commercial fluxes were determined from a sample of the 2-3 kg portion of the flux. The chemistries of Fluxes #1, #3 and #4 were determined by their components. A single sample was used to determine the pO_2 of the fluxes at various temperatures except for flux #20 where new flux samples were used each time. Using a single sample would minimize error caused by slightly varying composition from one sample to the next.

The basicity of each flux was calculated using the IIW's Basicity Index given earlier as Equation 5. The optical basicity was calculated using the method given in the Optical Basicity section. A sample calculation is given in Appendix A.

The EMF's of the oxygen probes were measured on a chart recorder. The readings typically stabilized in one or two minutes and remained relatively constant for one to two minutes longer, after which the probe was removed. The EMF response with time is plotted for each run in Figures 18 to 24. The oxygen pressure of each flux was measured at several temperatures ranging from 1650 to 1850 K. The results are summarized in Table 6 and shown graphically in Figure 17.

The EMF of the oxygen probes took one to two minutes to stabilize. This is substantially longer than the response times of the needle probes used by Janke (ref. 24) in liquid steel. He observed response times of less than 30 s at 1400 °C and that the response times decreased with increasing temperature. The response time in this study did not show any trends with temperature. Tube type oxygen probes used in steelmaking slags have shown similar response times as observed in this study. Some have found that a longer preheat time of the probe above the slag surface reduces the probe's response time (ref. 1). This would account for a lack of correlation with temperature as the preheat time in this study was only approximate and may have varied from five to ten minutes. Response times also depended on the flux. Fluxes #50, #91 and #3 all had relatively short response times, while fluxes #1 and #20 generally took longer to reach a stable EMF.

The life of the probe is defined as the length of time in which it maintains a stable EMF. The probe life will be different for each individual probe. This is especially true for plasma sprayed electrolytes because they will have considerable variation in their thickness. The slag may penetrate quickly in a thin area or at a defect in the coating. The probe life will also depend on the aggressiveness of the slag. The probes did not last long enough in flux #4 to reach a stable EMF; therefore no oxygen pressures were calculated for this flux. The probe life was generally longer at lower temperatures in all the fluxes used. The EMF remained stable for as short as 30 seconds in flux #20 while in most other fluxes the probes were removed before they failed.

Probe failure was observed as either a gradual decrease in the cell EMF or a suddenly erratic EMF output. In most cases the probes were removed after a stable EMF was achieved and before the probe deteriorated. The slow decrease in the cell EMF may be caused in part by oxygen transfer through the electrolyte as the slag penetrates it. This would polarize the cell reducing the oxygen gradient across it and thus reducing the cell's EMF.

The oxygen pressure was calculated from the cell EMF using Equation 19. The cell EMF also includes a contribution from the use of dissimilar metals (Mo and Pt6Rh) as electrodes. This modifies Equation 19 to include the thermoelectric effect (Et).

$$EMF = (RT/4F) \ln(pO_2(s)/pO_2(r)) + Et \quad (V) \qquad (29)$$

where EMF is in volts, R is the ideal gas constant, F is Faraday's constant, $pO_2(s)$ is the slag's oxygen pressure and $pO_2(r)$ is the reference oxygen pressure.

The potential for a Mo/Pt thermocouple has been recorded by others (ref. 21) as

$$Et = -22.1 + 0.040\ T \quad (mV) \qquad (30)$$

Since thermoelectric potentials are additive the potential for a Mo/Pt6Rh can be found by adding the potentials for a Mo/Pt and a Pt/Pt6Rh thermocouple. The data for a Pt/Pt6Rh thermocouple was estimated from the tables (ref. 34) for a Pt/Pt10Rh (S-type) thermocouple by interpolation between pure Pt and Pt10Rh. The following equation has been derived from this data for determining the Mo/Pt6Rh thermoelectric correction in the temperature range of 1600-1900 K.

$$Et = -18.7 + 0.033\ T \quad (mV) \qquad (31)$$

where T is in Kelvin.

The reference oxygen pressure used in this study was determined by the Mo/MoO_2 equilibrium. There is some conflict in the published values of this oxygen pressure, creating up to 10% difference between various authors' results. The value for the Mo/MoO_2 reference oxygen pressure used in this study is taken from the JANAF thermochemical tables (ref. 35).

$$\ln pO_2(Mo/MoO_2) = (-560369 + 160.037\ T) / RT \quad \text{.....(32)}$$

where R is the ideal gas constant in J/mol K and T the temperature in K and pO_2 in atm.

To calculate the oxygen pressure of the slag Equation 29 can be rearranged to

$$\ln pO_2(s) = \ln pO_2(r) + (4F/RT)\,[EMF - Et] \quad \text{.....(33)}$$

Substituting Equation 31 for Et, Equation 32 for $\ln pO_2(r)$ and inputting the values for the constants F and R we can directly calculate $\ln pO_2(s)$ from the temperature and cell potential.

$$\ln pO_2(s) = -68300/T + 20.8 + 46400\ EMF/T \quad (34)$$

where pO_2 is in atmospheres, T in Kelvin and EMF in Volts. A sample calculation is done in Appendix B.

The oxygen probes worked satisfactorily for all the fluxes except flux #4 (see composition Table 4). This flux was highly corrosive to the probes and the alumina sheathing on the Pt6Rh lead and on the thermocouple. The $ZrO_2(Y_2O_3)$ on the probes after the runs was cracked, very brittle and turned a dark or black color. With other fluxes the zirconia remained the same color as before the experiments or turned a slightly darker yellow color. The probable cause of the corrosiveness of this flux is the high CaF_2 content (over 17%). Although other fluxes had up to 10.0% CaF_2, they were not as corrosive as flux #4. All the other major components of this flux were present in higher amounts in other fluxes, except for Al_2O_3 which is a very stable oxide, thus is unlikely to be corrosive to the oxygen probes. The measurement of the oxygen pressure of several other fluxes with higher CaF_2 contents was attempted but these fluxes did not melt at 1873 K.

The oxygen pressure was found to increase linearly with the inverse of the temperature (T^{-1}), as shown in Figure 17. Although only three data points were measured for all the fluxes except #20, the correlations are quite good. Seven data points were taken on flux #20 and the correlation factor (r) of

ln pO_2 with T^{-1} is 0.93. Much of the scatter may be due to experimental error in measuring the oxygen probe EMF and the molten flux temperature. In addition possible electronic conduction, cell polarization and chemistry variations between samples used for chemical analysis and those used for pO_2 measurements may contribute to the total error.

Each flux increased in pO_2 to a different extent with a given change in temperature. The ln pO_2 of flux #3 remained relatively constant over the temperature range 1660-1850K. Although the scatter from the straight line relationship is not more than expected, the low slope leads to a very low correlation factor. From the results of this study, it is possible to say the oxygen pressure of flux #3 remains relatively constant over the temperature range examined.

The most significant source of experimental error is the EMF measurements of the oxygen probes. In some cases the EMF did not reach a constant value and therefore an approximate value for the EMF had to be taken. In these cases the EMF may have been as far off as 10 to 20 mV from the actual cell EMF. Improvements on the cell design and the uniformity of the plasma sprayed ZrO_2 layer will help reduce this error. In the other cases where the EMF stabilized for a significant period of time a maximum error of 5 mV is reasonable for the equipment used.

C. DISCUSSION

The results of this study show that the pO_2 decreases linearly with the inverse of the temperature (T^{-1}). The correlation between T^{-1} and ln pO_2 is very good as can be seen in the plots in Figure 17. Much of the scatter in the results may be contributed to experimental error. The oxygen pressure was expected to increase with temperature since increasing temperature reduces the stability of all oxides. The unknown was to what extent did temperature increase the pO_2 of different fluxes. This was found to be different for each flux used in this study.

The pO_2 is related to free energy of formation by Equation 8 given earlier. We also know that

$$\Delta G = \Delta H - \Delta S\, T \quad \text{.....(35)}$$

If we substitute Equation 35 into Equation 8 and solve for ln pO_2 we get

$$\ln pO_2 = (\Delta H/R)\,(1/T) - \Delta S/R \quad \text{.....(36)}$$

Therefore the slope of the relationship between ln pO_2 and T^{-1} is equal to the heat of formation of the flux divided by the gas constant.

The fluxes used in this study can be divided into three groups based on the measured pO_2. Fluxes #91 and #20 had the lowest pO_2's measured. The pO_2 for these fluxes also increased faster with increasing temperature than

the pO_2 of the other fluxes. Both of these fluxes were $CaO-SiO_2$ based fluxes.

Flux #91 was the most basic of all the fluxes according to the OB and BI, thus was expected to give the lowest pO_2. From examining its composition, we see that it contains a large amount of CaO, which is a very stable oxide, and low concentrations of weak oxide. Thus, it is expected to give a low pO_2 from point of view of the relative stability of oxides comprising the flux. Although flux #91 has a substantially higher BI and OB than flux #20 it has only slightly higher pO_2. One reason for this may be the higher concentration of CaF_2 in flux #91, which can react with oxides in the flux and increase the oxide activity (ref. 36). Flux #91 also contains slightly higher concentration of weak oxides, the main one being Na_2O.

Flux #20 had a higher SiO_2 content than #91, resulting in a lower BI and OB as well as a higher pO_2. The pO_2 was not that much higher in flux #20 than #91. This is most likely due to the lower CaF_2 and Na_2O content of flux #20 as discussed above.

The pO_2 of fluxes #50 and #3 were also very similar to each other, although the pO_2 did not vary with temperature to the same extent for both fluxes. These fluxes were $MnO-SiO_2$ based fluxes which are known to give a high oxygen content in weld metal. MnO is a very weak oxide

thermodynamically and was expected to give a high pO_2. The scatter in the results of flux #3 suggests that there is little variation of pO_2 with temperature for this flux. It also indicates that there may be another factor affecting the pO_2 of this flux which has a greater influence than temperature. One factor could be the presence of two immiscible liquid phases, since this flux contains a significant amount of CaF_2. Whether or not two liquid phases were present at these temperatures was not determined because there were no provisions to rapidly remove samples from the furnace at high temperature. Each phase would have a different pO_2 when melted but would tend to reach an equilibrium with time. The pO_2 actually measured would depend on which phase the probe is immersed in and on the kinetics for the phases to reach equilibrium.

Flux #1 had an intermediate pO_2 between the other two groups of fluxes. The chemistry of this flux is more complex, containing significant amounts of Al_2O_3 and TiO_2 as well as SiO_2 and CaO. Both Al_2O_3 and TiO_2 are considered to be acid oxides and to increase the weld metal oxygen content as demonstrated by their inclusion in the denominator of the BI formula.

This flux contains considerably less CaO than the fluxes #20 or #91 but more than fluxes #3 or #50. The oxides used instead of CaO, TiO_2 and Al_2O_3 are less stable than CaO and therefore would give a higher pO_2.

A common concept used in steelmaking is the sulphide capacity of the slag, which is usually defined by the following equation (ref. 37):

$$Cs = (wt\%\underline{S})(pO_2/pS_2)^{(1/2)} \quad \text{.....(37)}$$

This parameter is based on the desulphurization reaction given earlier as Equation 15. From Equation 15, we see that the desulphurization of steel is assisted by a high slag basicity and a low oxygen pressure. For slags not containing any transition metal oxides there is a good correlation between basicity and Cs (ref. 37); thus Cs can be used as a measure of the basicity of the slag.

Sosinsky and Sommerville (ref. 37) have found that the Cs varies linearly with T^{-1}. Since Cs is related to the pO_2 of the slag (by Equation 37), it implies that the pO_2 of the slag may also vary linearly with T^{-1}, which is what the author has found from this study.

Sosinsky and Sommerville also found the Cs to change to a greater extent with a change in temperature for higher basicity slags. The fact that the present author has found that the fluxes with the lowest pO_2 changed pO_2 to the greatest extent with temperature seems to be indicative of the similar behavior of the Cs of slags. One difference is that in the present study there have been fluxes with similar pO_2 but which vary with temperature to different extents, such as flux #3 and #50. The Cs has a constant change with increasing T^{-1} for a specific basicity (ref. 37). This may be due to the fact that the Cs data was from simple slags containing no transition metal oxides whereas we used complex oxide mixtures. Since the determination of the effects of transition metal oxides on basicity is questionable, the effects of temperature on a slag containing transition elements may be different for different fluxes with the same basicity. The other difference between Cs and pO_2 is that the Cs was found to depend on temperature and basicity (ref. 37). The pO_2 of the flux depends on the strength of the oxides in the flux rather than the basicity.

The practical aspect of measuring the pO_2 of SAW fluxes is to be able to determine whether one flux will give up more oxygen to the weld metal than another flux. By examining the fluxes at steelmaking temperatures

(1600 °C), we can rate the fluxes from the most stable to the least stable: 91, 20, 1, 3, and 50. This order seems reasonable in view of the examination of the relative stability of the oxides in each flux.

If we extrapolate our data to generally accepted effective weld pool reaction temperatures (2200 °C), the order of the fluxes changes to: 1, 3, 91, 20, and 50 (see Figure 25). Although there is some uncertainty in extrapolating the data from this study to such a high temperature, there is also some question as to the weld pool reaction temperature. The temperatures have been derived by applying equilibrium thermodynamics to the welding reactions, disregarding the kinetics involved in the short thermal cycle. Depending on the method used and the reaction studied, effective weld pool reaction temperatures of 1520 °C to 2500 °C have been deduced (ref. 17). It is clear that reactions are actually occurring in the weld pool at temperatures from the melting point to the highest temperature experienced at the electric arc. The final oxygen content might depend on the low temperature properties of the flux rather than the equilibrium temperatures of the weld pool reactions. In either case, it is certain that temperature has a great effect on the pO_2 of fluxes.

The pO_2 of the fluxes studied did not show any correlation with either OB or BI as can be seen in Figures 26 and 27. At steelmaking temperatures (1600 °C), there appears to be a good relationship between ln pO_2 and the

OB of the fluxes. This correlation only occurs for a very limited temperature range and is lost at higher or lower temperatures. Since the OB parameter was developed mainly for a more accurate basicity determination of steelmaking slag, this relationship may show that the OB is a good indicator of basicity and pO_2. When the data is extrapolated to welding temperatures (2200 °C) there is no correlation between ln pO_2 and OB. Thus, it appears that the OB is only good in predicting the relative reactivity of fluxes or slags at steelmaking temperatures. This may be one reason why researchers have had trouble in applying steelmaking knowledge of slag behavior to welding fluxes.

We can compare the data from this study to the pO_2 measurements done on steelmaking slags (ref. 1,2). The pO_2 tends to be much higher in this study than those referenced above which use steelmaking fluxes in equilibrium with iron. The pO_2 of these fluxes is determined by the Fe/FeO equilibrium reaction. Pure FeO has a free energy of formation of approximately -300 kJ/mole O_2 at 1800 K, which gives us a ln pO_2 = -20. The pO_2 for any slag containing FeO in equilibrium with Fe will have to be less than that for pure FeO, that is less than -19.3. If there are no metallic components present then the pO_2 will depend on the interaction of the oxides and halides within the slag. The pO_2 will be higher than the equilibrium pO_2 for individual oxides, otherwise some of the oxides in the flux would be reduced to a metal.

To obtain an approximation of how much oxygen is actually available to be dissolved by the weld metal from the flux we can convert the pO_2 measurements to a weight percent oxygen in iron. Assume that an equal volume of flux is melted as iron. Also assume that the pO_2 is equal to, rather than proportional to, the mass fraction of oxygen in the slag which is available to be dissolved by the iron. The calculated %O in the iron at various temperatures is given in Table 7 and a sample calculation is given in Appendix C. Although this is a very crude calculation, it does give an idea of the difference in the oxygen available from the different fluxes in terms of possible weld metal oxygen content. Table 7 also shows that the temperature of the flux plays a great role in determining the weld metal oxygen content. It is important to note that the final weld metal oxygen content of any one weld will depend on many other factors than just the pO_2 of the flux. Some of these factors are the base metal and electrode chemistry, the presence of deoxidizers such as Al or Si, welding parameters, and many others.

Extensive thermodynamic calculations, for comparison with the measured pO_2, cannot be done on the fluxes used in this study. The reason is the lack of activity data on complex fluxes. We can repeat Eagar's (ref. 6) calculations of the theoretical weld metal oxygen content at 2000 °C for $CaO\text{-}SiO_2$ fluxes. He based the weld metal oxygen content on the equilibrium of the following reaction:

$SiO_2 = \underline{Si} + 2\underline{O}$ .....(38)

The equilibrium constant derived from thermodynamic data is (ref. 6):

$\log K = -28360/T + 10.61$ and .....(39)

$K = (\%\underline{Si})(\%\underline{O})^2 / a(SiO_2)$ .....(40)

There is no available data on the activity of SiO_2 in these particular fluxes therefore the weight percent of SiO_2 in each flux was used instead. The calculated %O is plotted in Figure 28 against ln pO_2. There is no trend between the calculated %O and the measured ln pO_2. The question of whether 2000 °C is the proper temperature to use also sheds doubt on this comparison. A more extensive study on the pO_2 of fluxes is needed to determine if it a better predictor of weld metal oxygen content than that proposed by Eagar.

From a detailed statistical analysis of the data in this study we have found an excellent correlation between the pO_2 of the fluxes and the molar percents of CaO, SiO_2, CaF_2 and MnO. Since we only have pO_2 data from five fluxes we can only perform a regression analysis on three variables at once. For this reason CaO and CaF_2 were grouped together. This gave a

slightly higher correlation factor than using either component alone. In fact, the correlation factor (r) at 1600 °C was 1.000. Even at 2200 °C, based on the extrapolated ln pO_2 data, the correlation factor was 0.996. The calculations are shown in Appendix D. The effect that each of these oxides has on the pO_2 depends significantly on the temperature. Each oxide's effect changes to a different extent with temperature. From our analysis given in Appendix D we can write the formula:

$$\ln pO_2 = A\,(CaO+CaF_2) + B\,SiO_2 + C\,MnO + D \quad (41)$$

The coefficients depend on temperature according to the following formulas:

$$A = 1.0905 - 2268.7/T \quad (42)$$

$$B = 1.0717 - 2112.4/T \quad (43)$$

$$C = 0.3657 - 468.06/T \quad (44)$$

$$D = -66.219 + 112866/T \quad (45)$$

From this formula we can calculate the ln pO_2 of any of the fluxes at any temperature range. Future pO_2 measurements on other fluxes will prove if this relationship will hold for a wide range of flux types, or only for the types of fluxes used in this study.

The excellent correlation found in the above formula raises the question as to why only CaO, CaF_2, SiO_2 and MnO have an effect on the pO_2 of the fluxes. Additional pO_2 data, on a wide variety of fluxes, may indeed show that certain other oxides must be taken into account, but the high correlation factor indicates that these oxides are the most significant in determining the pO_2 of the fluxes used in this study.

The measurement of the pO_2 of fluxes may provide a very useful tool in development of future fluxes for SAW. This approach provides a method of directly analysing, by measurement, the oxygen potential of fluxes and reduces our reliance on empirical formulae and room temperature properties. It also provides an alternative approach than the vague concept of basicity and its questionable relationship to the weld metal oxygen content. The trends of pO_2 with temperature and the relationship between pO_2 and weld metal oxygen content will allow fluxes to be developed with low pO_2 at welding temperatures. It would be desirable to have fluxes with relatively low pO_2 which does not change significantly with temperature. The effects of different oxides on both the pO_2 and its dependence on temperature will show flux developers which oxides to use for the desired effect, with less emphasis on the trial and error method which we now rely upon.

D. CONCLUSIONS

1. Disposable oxygen probes were constructed by plasma spraying a stabilized zirconia coating over a molybdenum wire. These probes were successfully used to measure the oxygen pressure of submerged arc welding fluxes over the temperature range of 1400 °C to 1600 °C. The Y_2O_3-stabilized zirconia was found to withstand attack from the slag better than CaO-stabilized probes.

2. The measured pO_2 of the fluxes were found to correlate well with the stability of the component oxides and to the optical basicity of the fluxes at steelmaking temperatures. However, a poor correlation was found with the basicity index recommended by the International Institute of Welding.

3. Extrapolating the data to higher temperatures (2200 °C) changes the relative stability of the fluxes and contradicts the correlations found at lower temperatures between oxygen pressure and oxide stability or optical basicity. Oxides which tend to cause the pO_2 of a flux to remain constant with increasing temperature may be more useful in developing low oxygen potential fluxes than the traditional stable oxides such as CaO.

4. Statistical analysis shows a close relationship between the oxygen pressure and the molar concentrations of CaF_2, CaO, SiO_2 and MnO in the fluxes. An equation to describe the relationship between these concentrations and the temperature has been developed which is:

$$\ln pO_2 = A\,(CaO+CaF_2) + B\,SiO_2 + C\,MnO + D \quad \text{.....(39)}$$

where,

$$A = 1.0905 - 2268.7/T \quad \text{.....(40)}$$

$$B = 1.0717 - 2112.4/T \quad \text{.....(41)}$$

$$C = 0.3657 - 468.06/T \quad \text{.....(42)}$$

$$D = -66.219 + 112866/T \quad \text{.....(43)}$$

	BASICITY RATIOS	YEAR
1:	$\frac{\%O \text{ (from MeO)}}{\%O \text{ (from } SiO_2)}$	1896
2:	$\frac{\%MeO}{\%SiO_2 + \%Al_2O_3}$	1892
3:	$\frac{\%CaO}{\%SiO_2}$	1901
4:	$\frac{MeO - 3\ P_2O_5}{SiO_2}$	1922/1923
5:	$\%CaO - 1.86\ \%SiO_2 - 1.19\ \%P_2O_5$	1934
6:	$\frac{CaO - 4\ P_2O_5}{SiO_2}$	1942
7:	$MeO - 2\ SiO_2 - 4\ P_2O_5 - 2\ Al_2O_3 - Fe_2O_3$	1946
8:	$\frac{MeO}{SiO_2 + 2\ P_2O_5 + 0.5\ Al_2O_3 + 0.5\ Fe_2O_3}$	1946
9:	$\frac{\%CaO}{\%SiO_2 + \%P_2O_5}$	1947
10:	$CaO + 2/3\ MgO - SiO_2 - Al_2O_3$	1949
11:	$\frac{\%CaO + \%MgO}{\%SiO_2 + 0.6\ \%Al_2O_3\ \frac{(\%CaO + \%MgO - 1.19)}{\%SiO_2}}$	1956
12:	$\frac{\%CaO + 0.7\ \%MgO}{0.94\ \%SiO_2 + 0.18\ \%Al_2O_3}$	1960
13:	$\frac{\%CaO + \alpha\ \%MgO + 2.0\ \%MnO}{\%SiO_2 + 0.6\ \%Al_2O_3\ \frac{(\%CaO + \alpha\ \%MgO - 1.19)}{\%SiO_2}}$ where $\alpha = \frac{1.84\ \%SiO_2 - 0.9\ \%CaO}{\%SiO_2 + 0.9\ \%MgO}$	1962

Table 1: Examples of some Basicity Ratios of slags used in steelmaking. (M.G. Frohberg and M.L. Kapoor, "The Application of a New Basicity Index to Metallurgical Reactions." Stahl und Eisen, 91 No. 4, (1971), pp. 183.)

$$\log \frac{Fe^{2+}}{Fe^{3+}} = a + \frac{b(1)}{(T)} + c \log pO_2$$

Workers	Coefficients			Multiple Correlation Coefficient
	a	b	c	
Johnston	1.927	-5332.5	-0.232	0.998
Tran&Brungs	-0.5514	-1974.2	-0.254	0.985
Combined Data	1.791	-5131.3	-0.236	0.995

Table 2: Relationship between Fe^{2+}/Fe^{3+} and oxygen pressure of sodium disilicate glass (ref. 27).

Arc Current (amps)	900
Arc Gas (psi)	50
Aux Gas (psi)	100
Powder Gas (psi)	40
Powder Feed Rate	3.2
Spray Distance (in)	3
Preheat Temp. (C)	23
# of Passes	11

Table 3: Plasma spray parameters for application of $ZrO_2(Y_2O_3)$.

	ZrO2(CaO)	ZrO2(Y2O3)
ZrO2	92.99	88.994
CaO	5.37	0.064
MgO	0.59	0.180
Y2O3	----	7.660
HfO2	----	< 2.5
TiO2	0.15	0.150
Al2O3	0.17	0.098
SiO2	0.54	0.220
Fe2O3	0.19	0.091
U+Th	----	0.043

Table 4: Composition of solid electrolytes.

	1	3	20	50	91	4
Na2O	1.73	1.86	0.20	0.40	5.25	1.59
MgO	0.00	17.28	9.16	0.54	2.04	11.91
Al2O3	12.23	1.72	4.66	4.40	4.59	32.34
SiO2	31.69	48.68	58.50	43.27	37.45	10.45
K2O	0.78	0.10	0.11	0.52	0.14	0.01
CaO	15.57	0.72	22.90	8.96	33.92	0.64
TiO2	25.23	0.00	0.18	0.69	3.72	11.99
MnO	0.00	22.12	0.00	35.95	0.23	0.91
FeO	0.76	0.96	0.24	2.19	0.19	0.82
ZrO2	0.51	0.00	0.00	0.00	0.00	0.22
CaF2	10.00	6.15	3.80	2.79	9.85	17.17
OB	0.616	0.568	0.594	0.559	0.675	0.637
BI(IIW)	0.56	0.76	0.6	0.71	1.24	0.89

Table 5: Composition of the Submerged Arc Welding fluxes.

Flux #	Temp (K)	ln pO2
1	1650	-13.5
	1750	-12.7
	1830	-11.6
3	1660	-7.5
	1710	-8.1
	1850	-7.2
20	1640	-17.7
	1660	-17.6
	1700	-15.2
	1760	-14.1
	1760	-14.0
	1800	-14.6
	1850	-13.0
50	1680	-8.0
	1750	-7.9
	1860	-6.2
91	1680	-18.1
	1750	-17.1
	1840	-14.2

Table 6: Calculated ln pO_2 values from EMF reading of the oxygen probes.

Temp (K)	Flux #1	Flux #3	Flux #20	Flux #50	Flux #91
1800	1.86E-04	1.84E-02	3.24E-05	3.17E-02	6.50E-06
2000	1.05E-03	2.79E-02	1.41E-03	1.79E-01	3.94E-04
2200	4.33E-03	3.93E-02	3.09E-02	7.36E-01	1.13E-02
2400	1.41E-02	5.23E-02	4.04E-01	2.36E+00	1.86E-01

Table 7: Theoretical percent oxygen in iron if it is melted with an equal volume of flux.

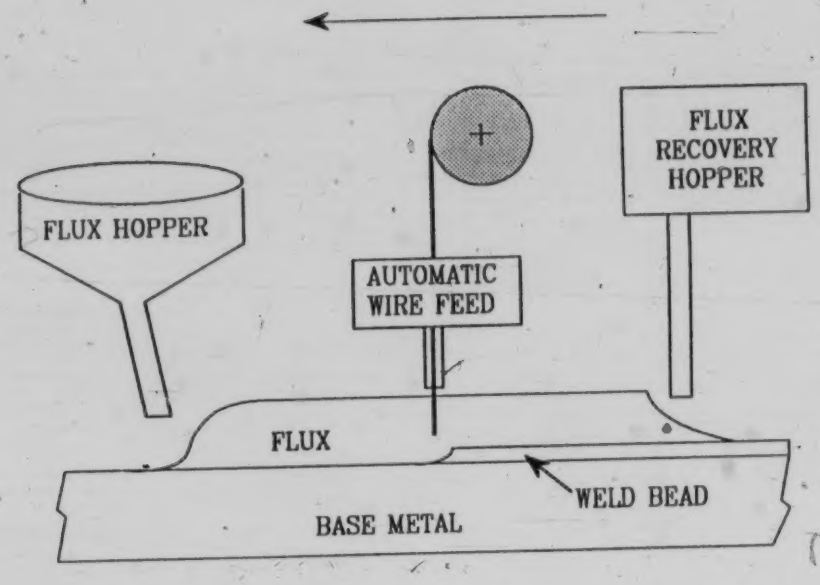

Figure 1: Schematic of SAW process.

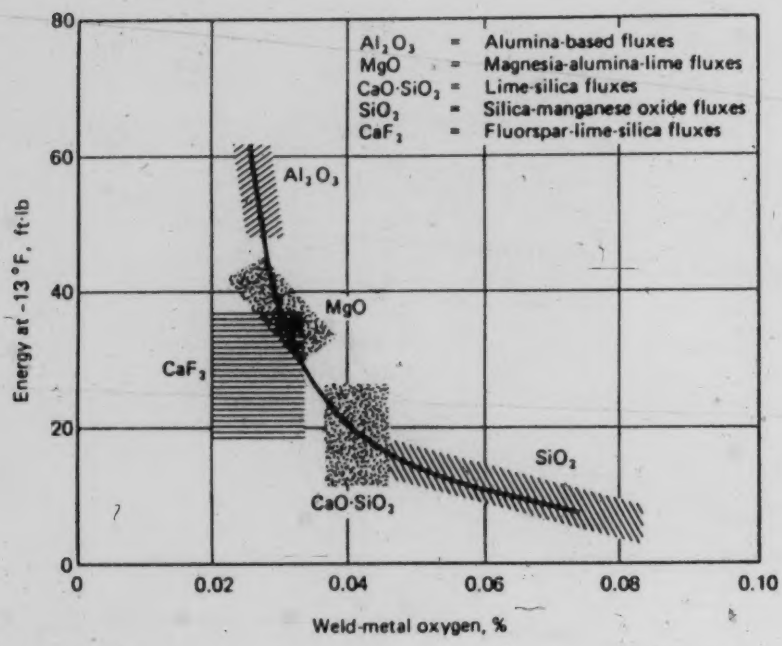

Figure 2: Typical Charpy V-notch toughness and weld metal oxygen content for different flux types (ref. 3).

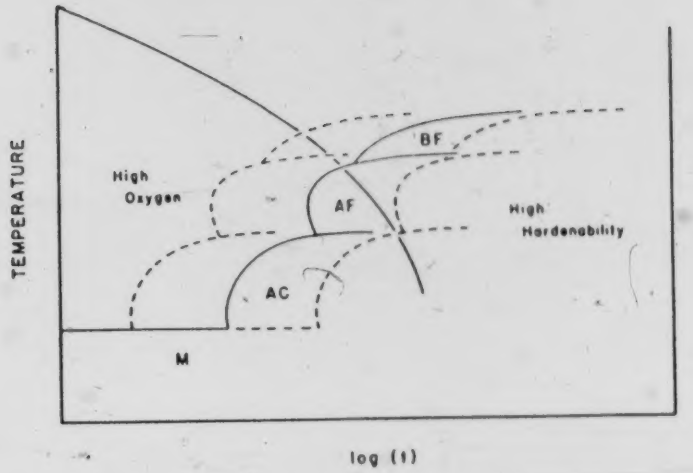

Figure 3: Cooling curve for a low carbon, low alloy steel showing the effects of oxygen content. M=Martensite, AC=Aligned ferrite with carbide (upper bainite), AF=Acicular ferrite and BF=Blocky ferrite (ref. 4).

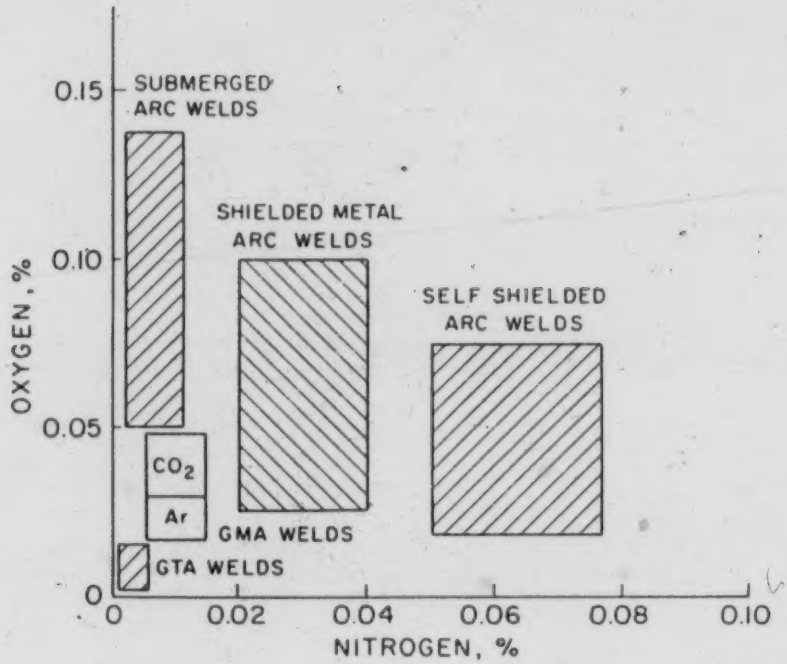

Figure 4: Typical oxygen and nitrogen content of weld metal for different welding processes (ref. 16).

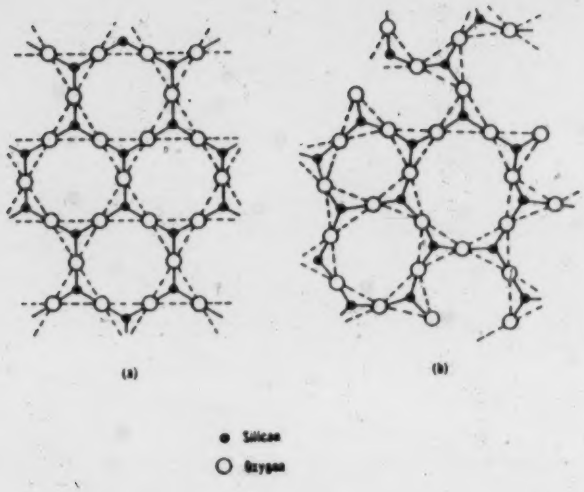

Figure 5: Structure of a) crystalline and b) molten silica (ref. 9).

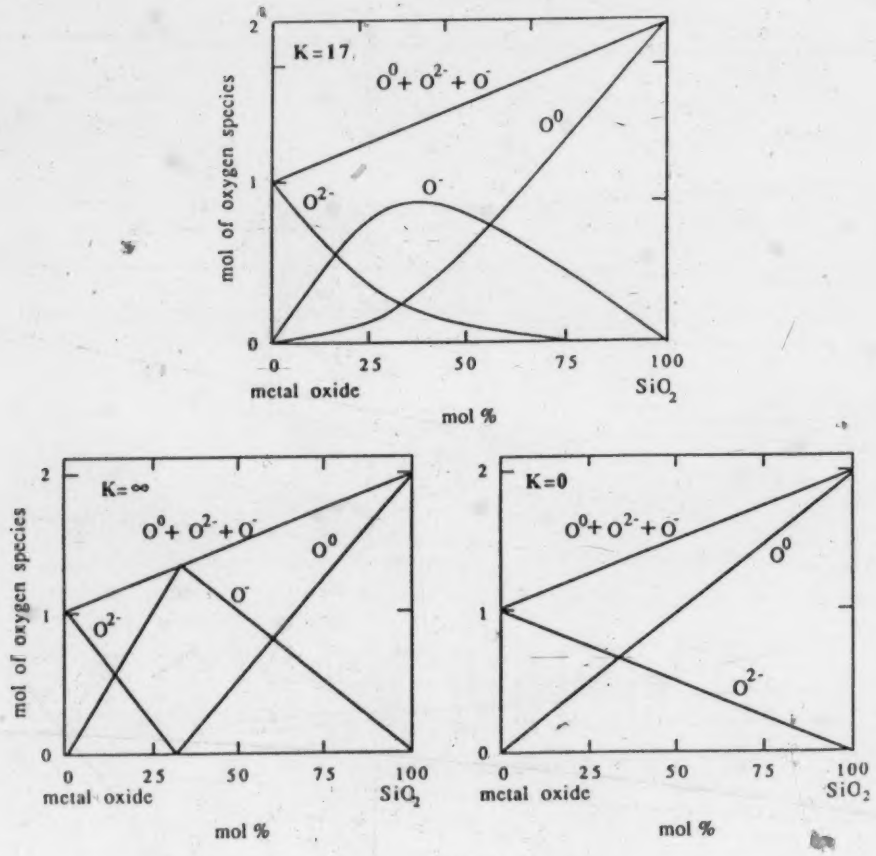

Figure 6: Theoretical concentration of bridging (O^0), non-bridging (O^{1-}) and free (O^{2-}) oxygen for different values of the equilibrium constant (K). (E.T. Turkdogan, Physiochemical Properties of Molten Slags and Glasses, Metals Society, London, 1983, p. 52)

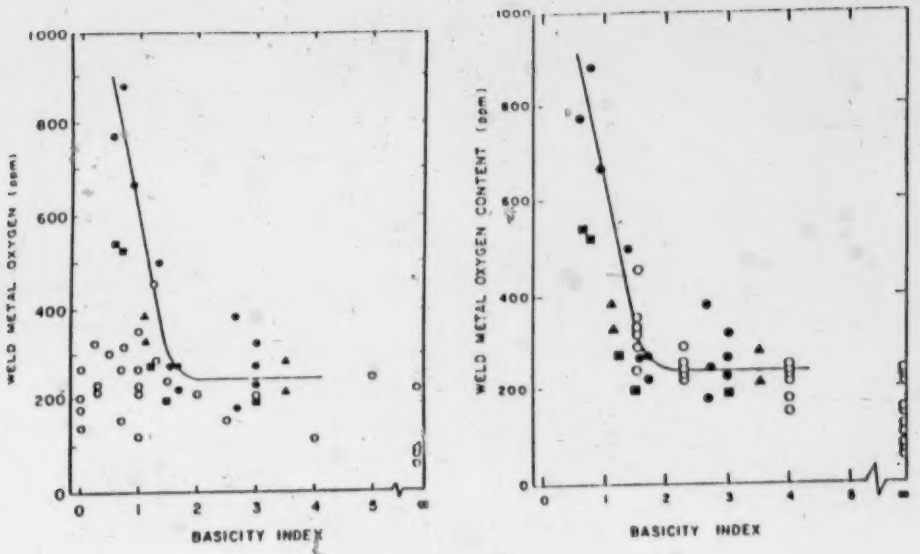

Figure 7: Basicity Index (IIW) versus weld metal oxygen content (réf. 4).
a) without CaF_2 term
b) with CaF_2 term.

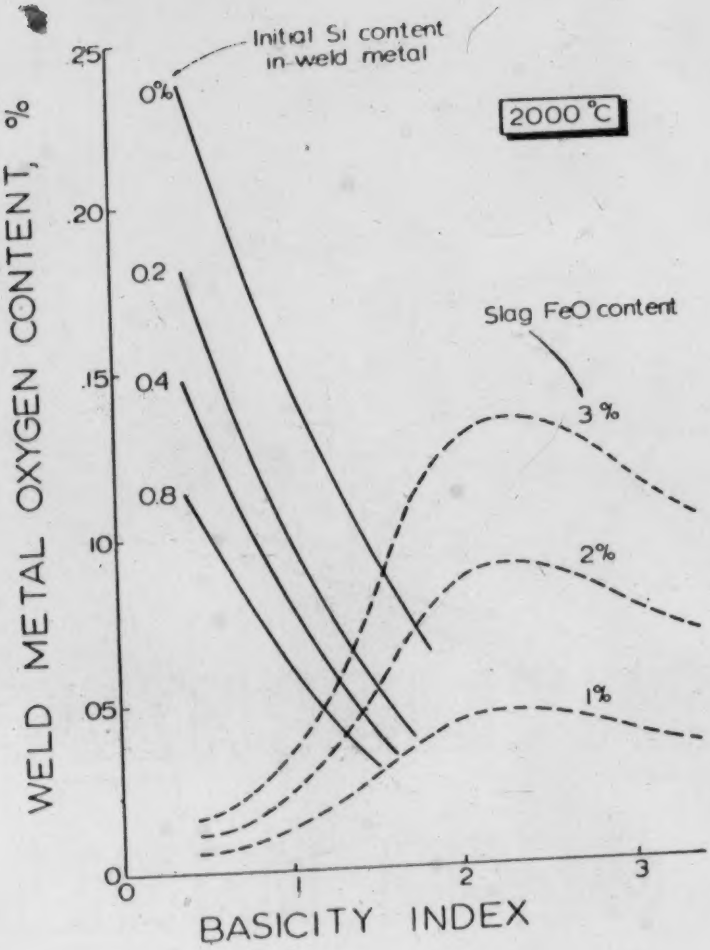

Figure 8: Dissolved oxygen equilibrium based on the SiO_2 and the Fe_xO reactions as a function of basicity for SiO_2-CaO-FeO slags (ref. 6).

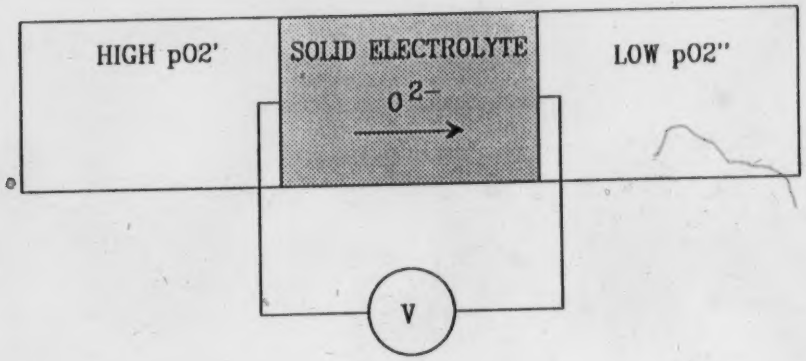

$$EMF = \frac{RT}{4F}(\ln pO2' - \ln pO2'')$$

Figure 9: Schematic of an oxygen concentration cell.

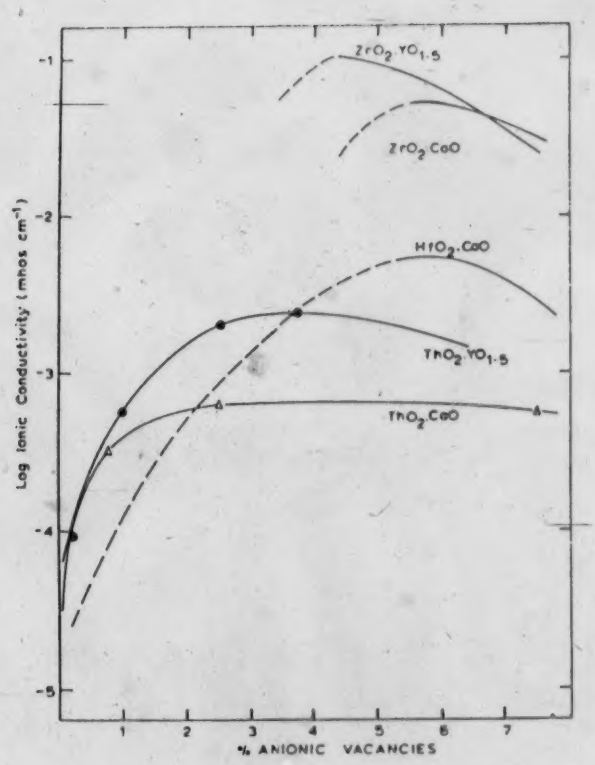

Figure 10: Ionic conduction of different solid electrolytes as a function of percent anion vacancies. (E.C. Subbarao, Editor, Solid Electrolytes and Their Application, Plenum Press, New York, 1980, p. 6.)

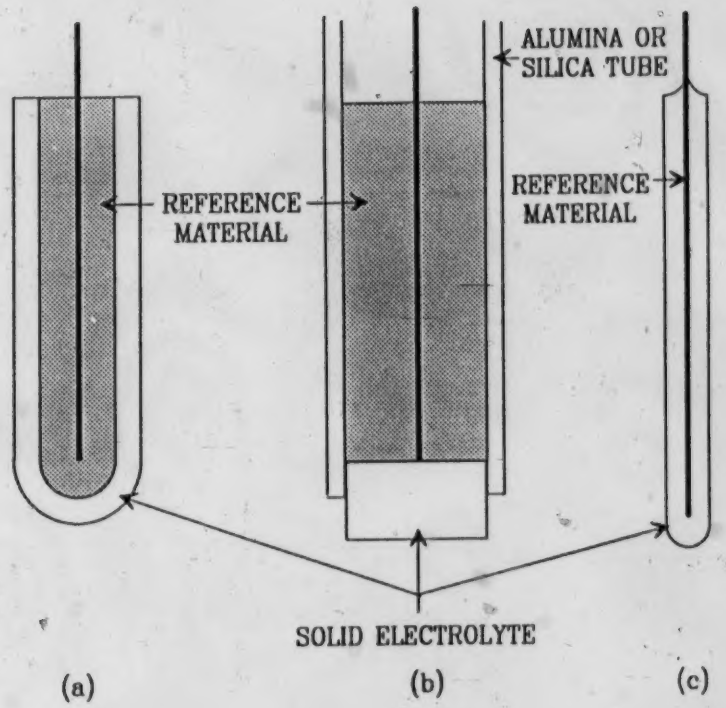

Figure 11: Common types of oxygen probes. (a)Tube type (b)Plug type and (c)Needle type.

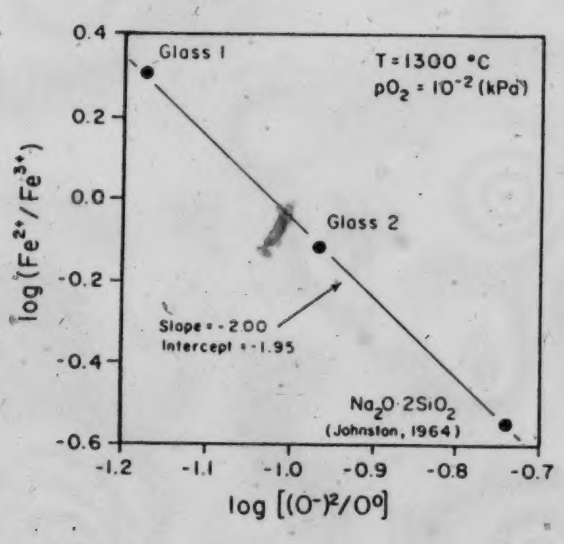

Figure 12: Oxidation state of iron as a function of basicity (ref. 28).

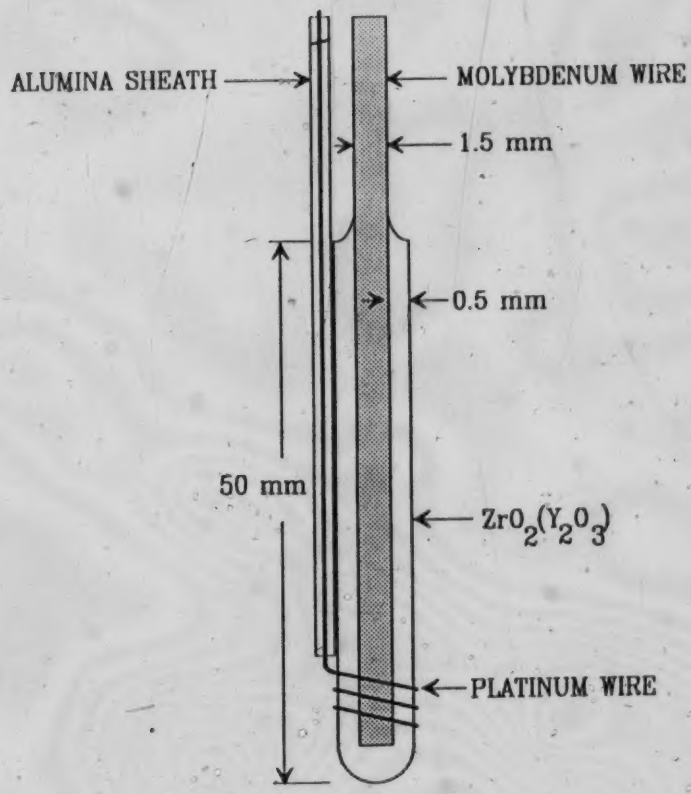

Figure 13: Schematic of needle probe used in this study.

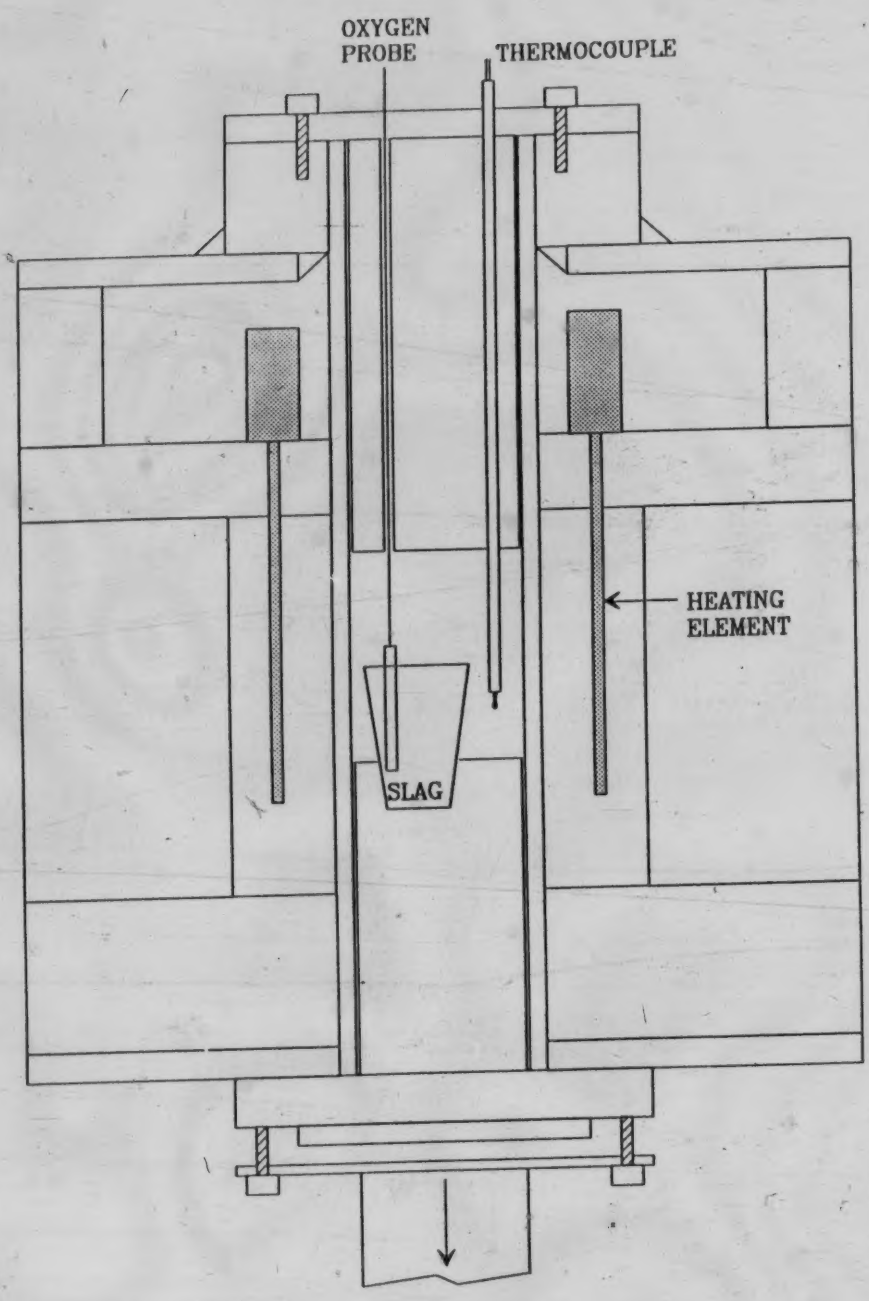

Figure 14: Schematic of furnace used in this study.

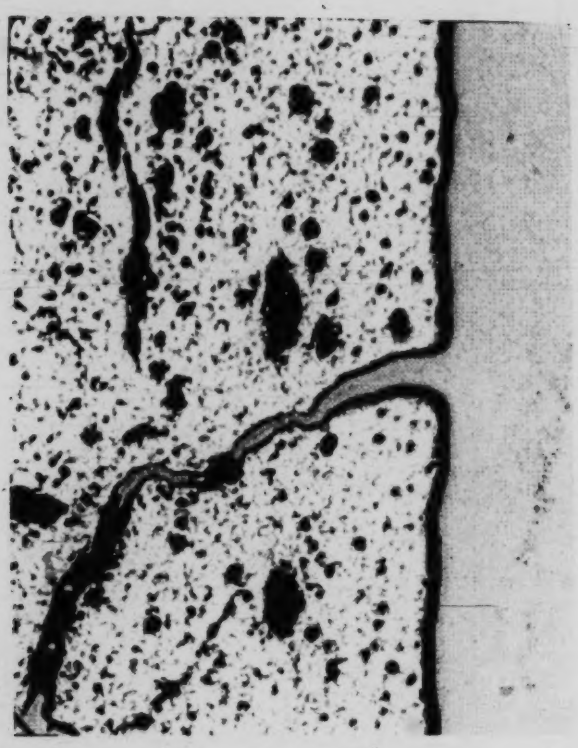

Figure 15: Cross section of used $ZrO_2(CaO)$ probe.

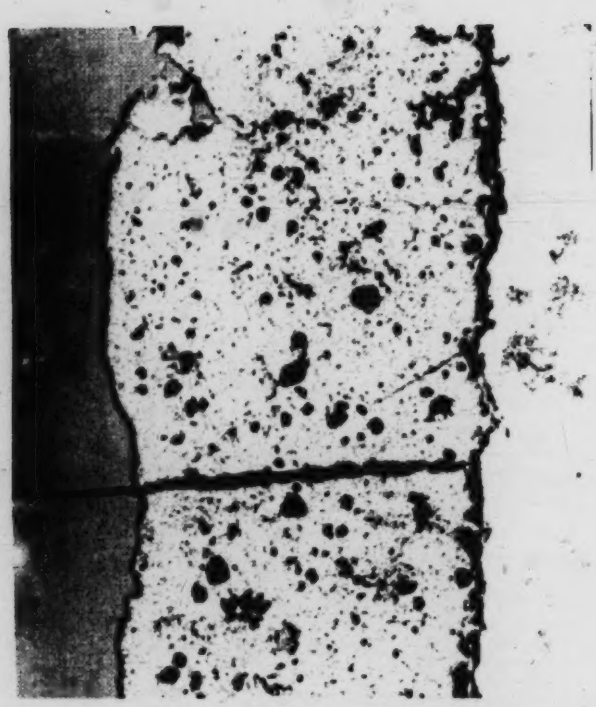

Figure 16: Cross section of used $ZrO_2(Y_2O_3)$ probe.

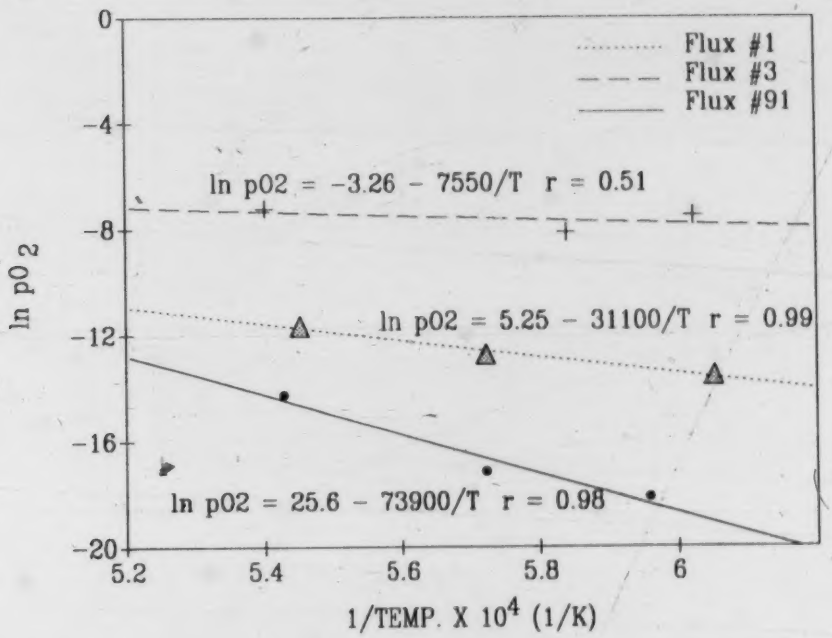

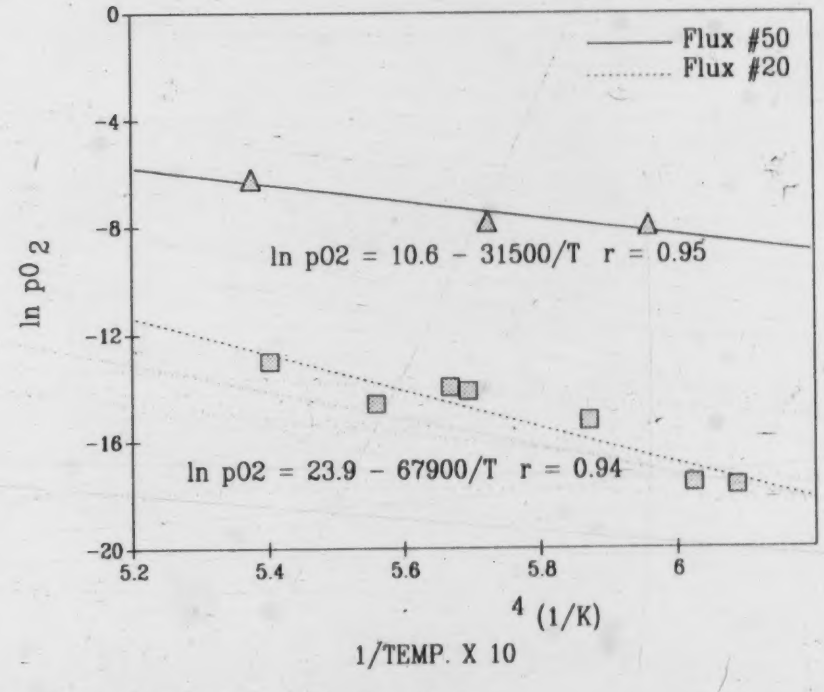

Figure 17: ln pO_2 versus 1/temperature.

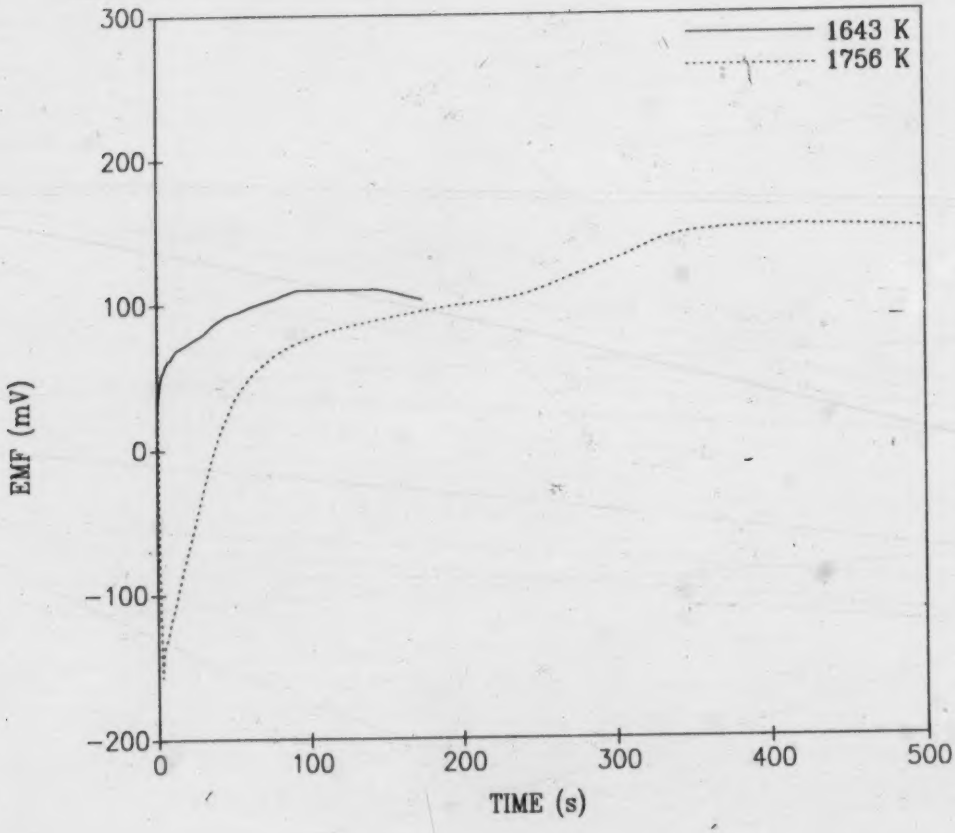

Figure 18: Oxygen probe's EMF response for flux #20 using the $ZrO_2(CaO)$ probes.

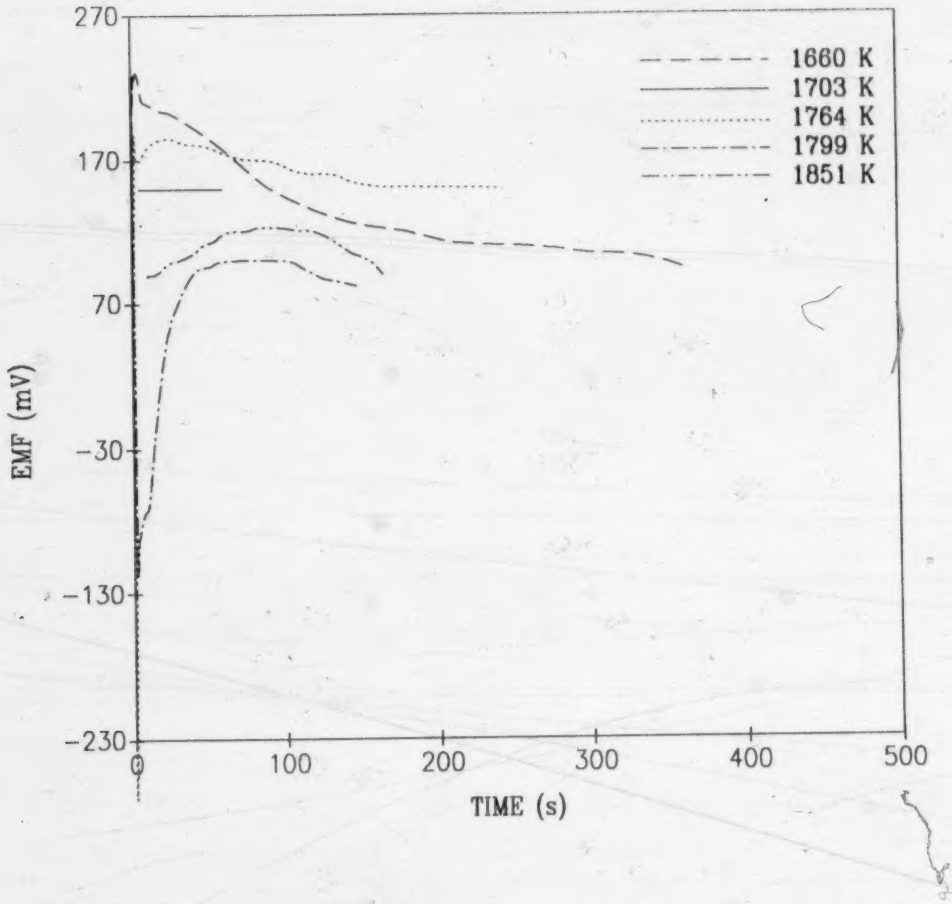

Figure 19: Oxygen probe's EMF response for flux #20 using the ZrO2(Y2O3) probes.

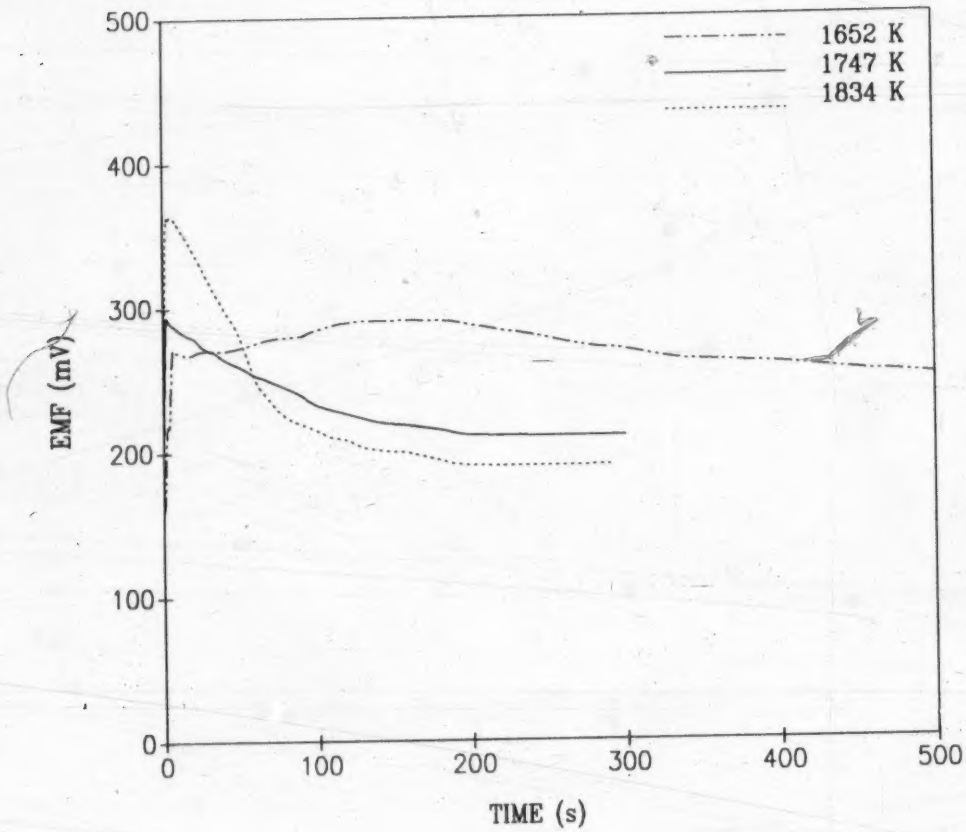

Figure 20: Oxygen probe's EMF response for flux #1 using the $ZrO_2(Y_2O_3)$ probes.

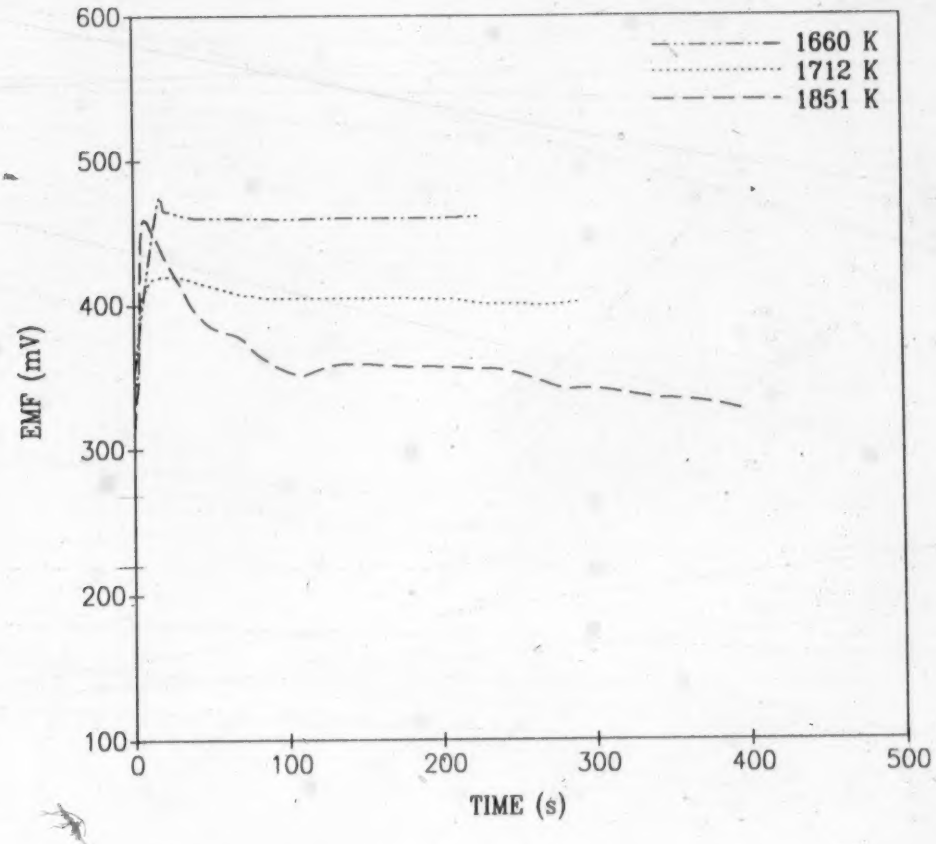

Figure 21: Oxygen probe's EMF response for flux #3 using the $ZrO_2(Y_2O_3)$ probes.

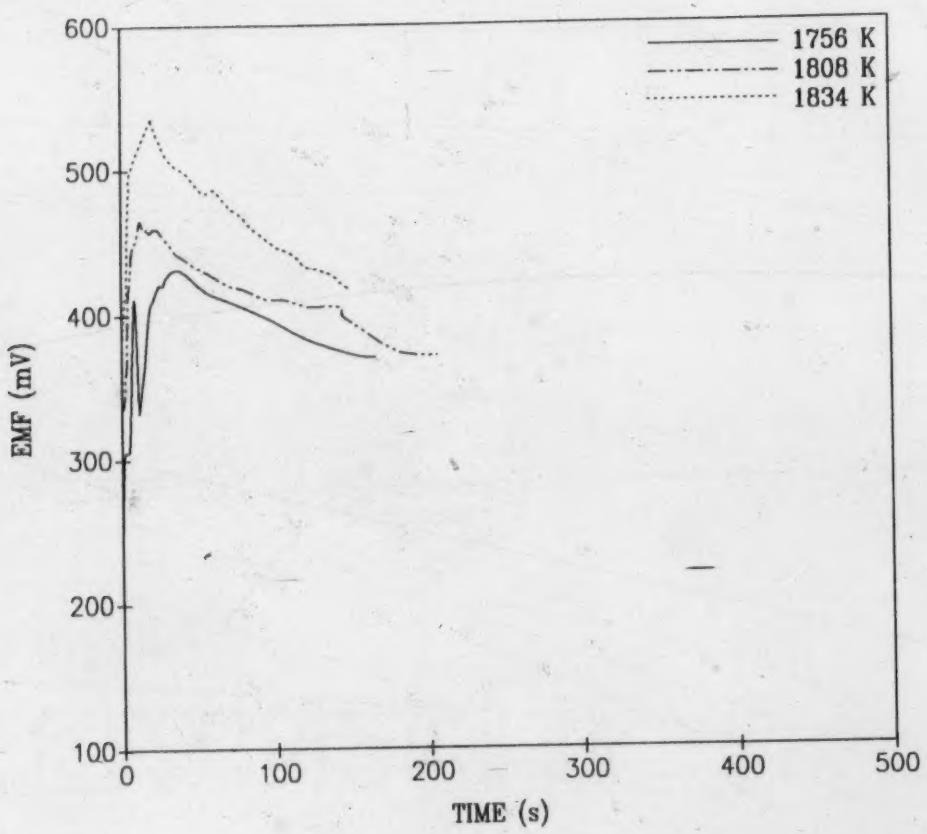

Figure 22: Oxygen probe's EMF response for flux #4 using the $ZrO_2(Y_2O_3)$ probes.

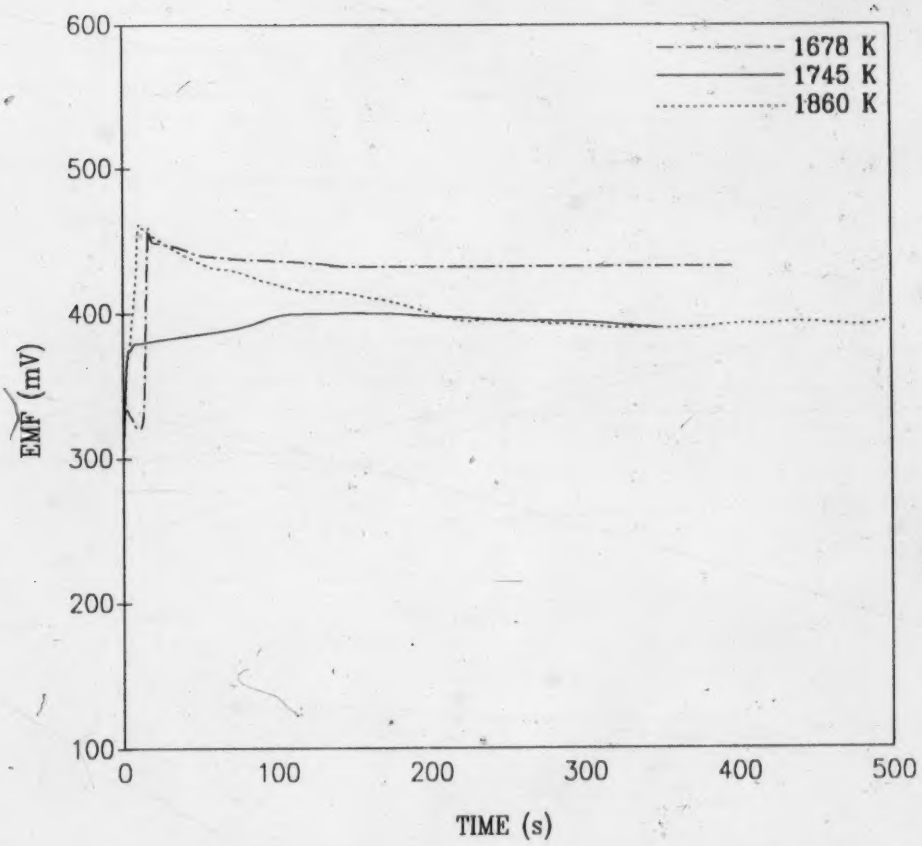

Figure 23: Oxygen probe's EMF response for flux #50 using the $ZrO_2(Y_2O_3)$ probes.

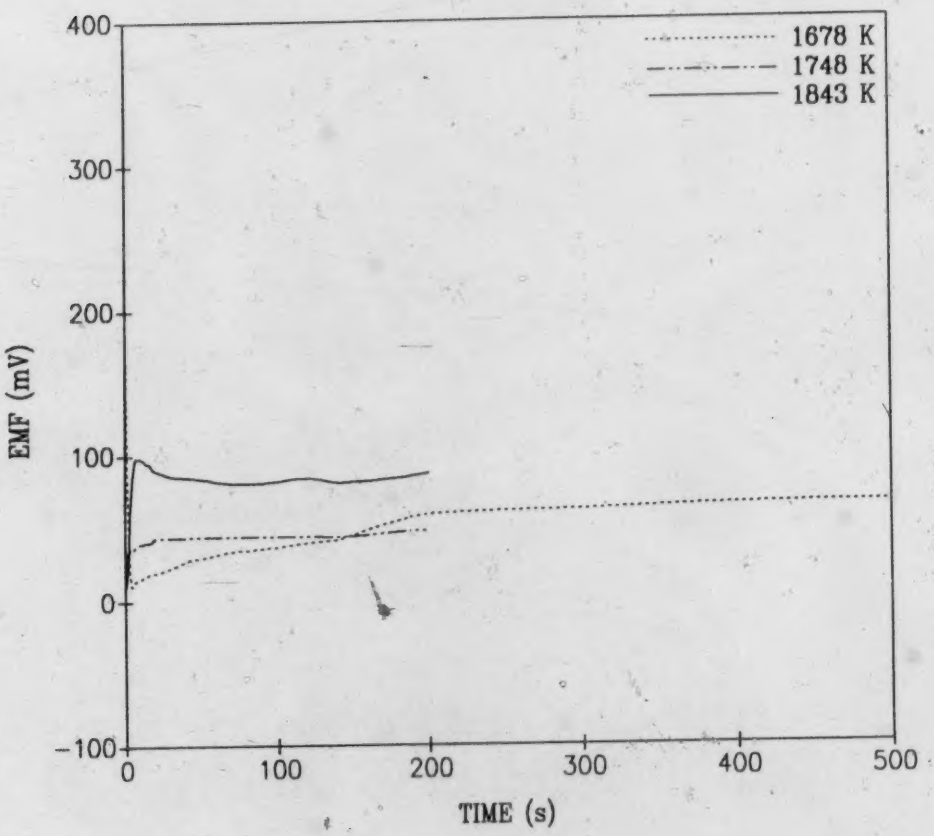

Figure 24: Oxygen probe's EMF response for flux #91 using the $ZrO_2(Y_2O_3)$ probes.

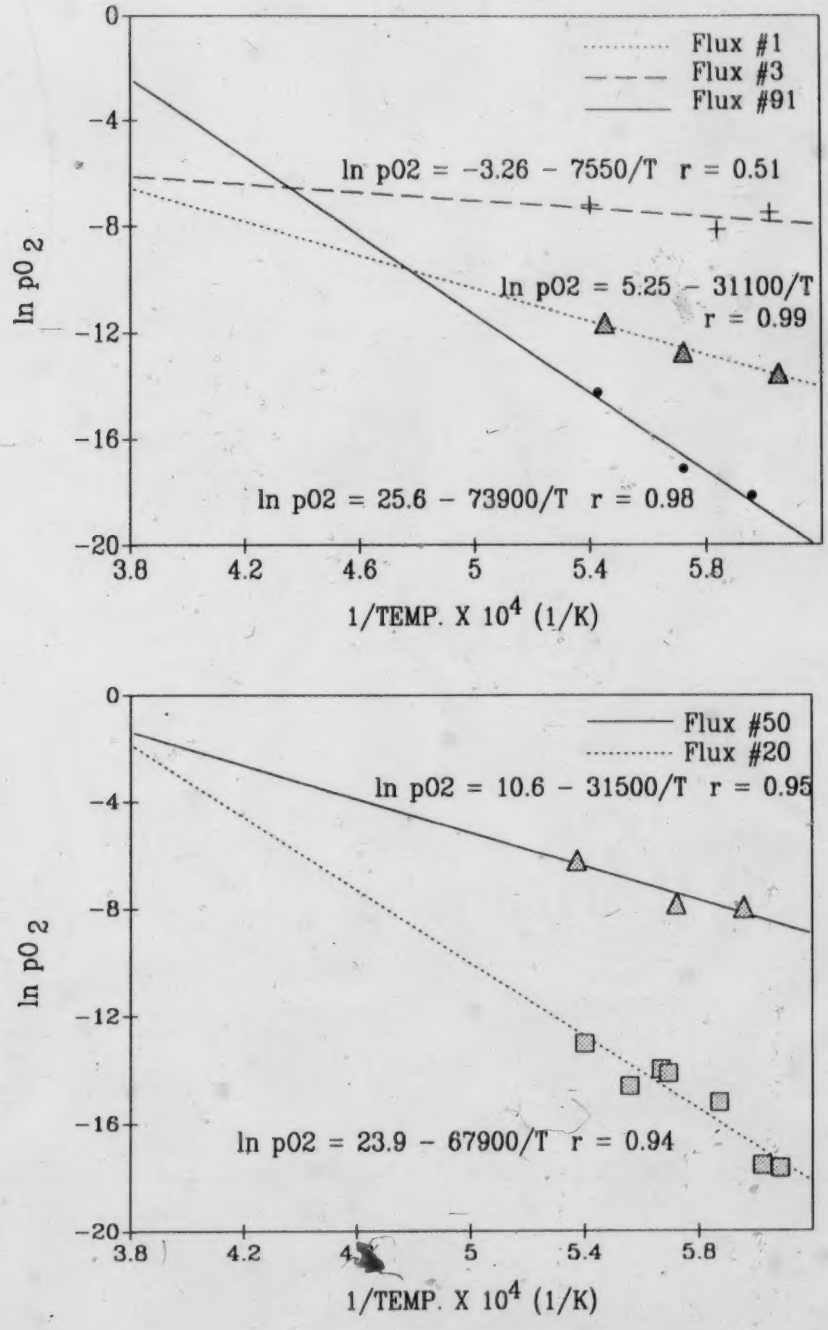

Figure 25: ln pO_2 versus 1/temperature, extrapolated to 2600 K.

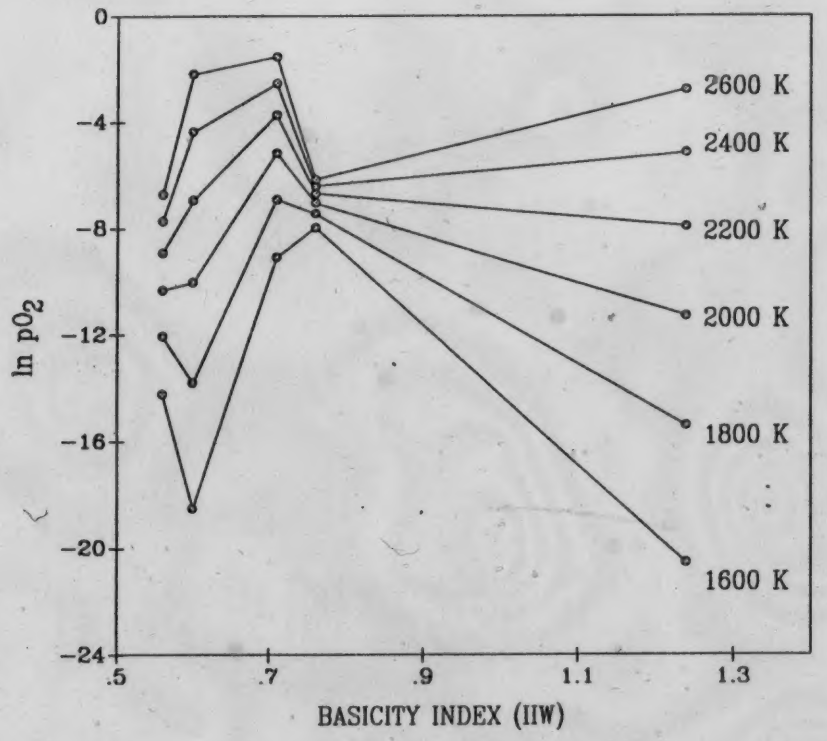

Figure 26: ln pO_2 versus Basicity Index (IIW) at various temperatures.

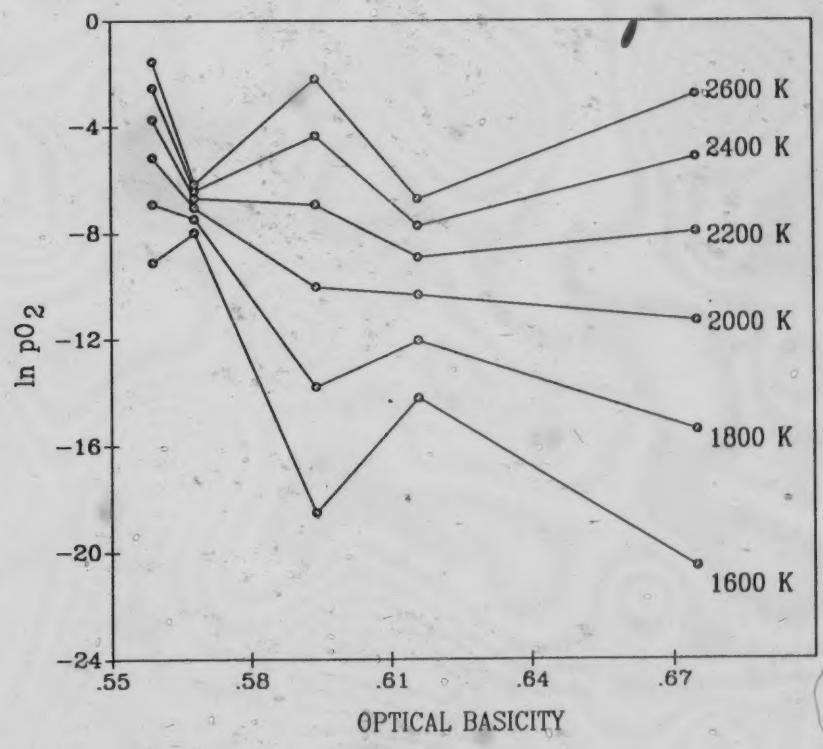

Figure 27: In pO_2 versus Optical Basicity at various temperatures.

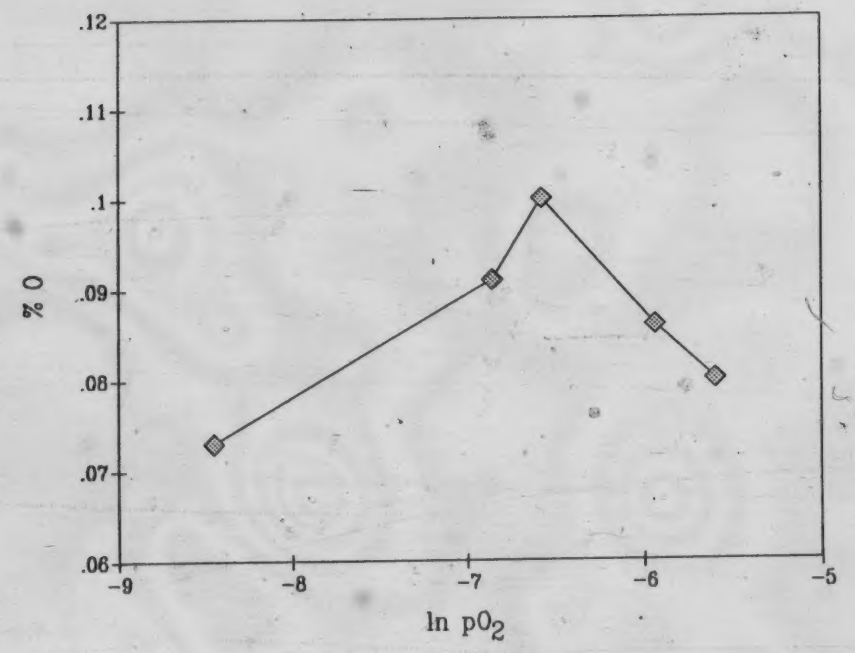

Figure 28: ln pO_2 versus theoretical percent oxygen in the weld metal using the method for calculations from Eagar (ref. 6).

REFERENCES

1. M. Kawakami, K.S. Goto and M. Matsuaka, "A Solid Electrolyte Oxygen Sensor for Steeelmaking Slags of the Basic Oxygen Converter." Metallurgical Transactions B, 11B, (1980) pp.463-469.

2. M. Iwase, N. Yamada, K. Nishida and E. Ichise, "Rapid Determination of the Activities in CaO-Fe_xO Liquid Slags by Disposable Electrochemical Oxygen Probes." ISS Transactions, 4, (1984), pp. 69-75.

3. American Society for Metals, Metals Handbook, 9th Ed., Vol. 6, ASM International, Metals Park Ohio, (1983), pp. 114-152.

4. C.B. Dallam, S. Liu and D.L. Olson, "Flux Composition Dependence of Microstructure and Toughness of Submerged Arc HSLA Weldments." Welding Journal, (1985), pp. 140s-151s.

5. T. Lau, G.C. Weatherly and A. McLean, "The Sources of Oxygen and Nitrogen Contamination in Submerged Arc Welding Using CaO-Al_2O_3 Based Fluxes." Welding Journal, (1985), pp. 343s-347s.

6. T.W. Eagar, "Sources of Weld Metal Oxygen Contamination During Submerged Arc Welding." Welding Journal, (1978), pp. 76s-80s.

7. N. Christensen and O. Grong, "Reactions of Acid and Weakly Basic Submerged-Arc Fluxes." Scandinavian Journal of Metallurgy, 13, (1986), pp. 30-40.

8. T. Lau, G.C. Weatherly and A. McLean, "Gas/Metal/Slag Reactions in Submerged Arc Welding Using CaO-Al_2O_3 Based Fluxes." Welding Journal, (1986), pp. 31s-38s.

9. J.D. Gilchrist, Extraction Metallurgy, 3rd Ed., Pergamon Press, New York, 1989, pp. 194-195.

10. B.O. Mysen, Structure and Properties of Silicate Melts, Elsevier, New York, 1988.

11. S.S. Tuliani, T. Boniszewski and N.F. Eaton, "Notch Toughness of Commercial Submerged Arc Weld Metal." Welding and Metal Fabrication, 37, (1969), pp. 327-339.

12. J.A. Duffy and M.D. Ingram, "Establishment of an Optical Scale for Lewis Basicity in Inorganic Oxyacids, Molten Salts and Glasses (Part 1)." Journal of the American Chemical Society, 93, pp. 6448-6454.

13. J.A. Duffy, M.D. Ingram and I.D. Sommerville, "Acid-Base Properties of Molten Oxides and Metallurgical slags." Journal of the Chemical Society, Faraday Transactions I, 14, (1978), pp. 1410-1419.

14. I.D. Sommerville, "Optical Basicity of Metallurgical Slags." Unpublished Document.

15. J.D. Gilchrist, Extraction Metallurgy, 3rd Ed., Pergamon Press, New York, 1989, p. 150.

16. C.S. Chia and T.W. Eagar, "Slag Metal Reactions in Binary CaF_2-Metal Oxide Welding Fluxes." Welding Journal, (1982), pp. 229s-232s.

17. T.H. North, H.B. Bell, A. Nowicki and I. Craig, "Slag/Metal Interaction, Oxygen and Toughness in Submerged Arc Welding." Welding Journal, (1978), pp. 63s-75s.

18. C. Wagner, "The Concept of the Basicity of Slags." Metallurgical Transactions B, 6B, (1975), pp. 405-409.

19. K.C. Mills, "The Physiochemical Properties of Slags, Part V. A Review of the Phase Diagrams for CaF_2 Based Slags." National Physical Laboratory Report, Chem 100, July 1979.

20. F.A. Kroger and H.J.Vink, "Solid State Physics", E. Seitz and D. Turnbull, Eds., Vol. 3, Academic Press, New York, 1956, p. 310.

21. M. Iwase, E. Ichise, M. Takeuchi and T. Yamasaki, "Measurements of the Parameter, $P\Theta$, for the Determination of Mixed Ionic and n-type Electronic Conduction in Commercial Zirconia Electrolytes." Transactions of the Japan Institute of Metals, 25, (1984), pp. 43-52.

22. B. Cales and J.F. Baumard, "Oxygen Semipermeability and Electronic Conductivity in Calcia-Stabilized Zirconia." Journal of Material Science, 17, (1982), pp. 3243-3248.

23. M.J.U.T. van Wijngaurchen, J.M.A. Geldenhuis and R.J. Dippenaar, "A Quantitative Assessment of Mixed Ionic and Electronic Conduction in Some Commercially Available Magnesia-Stabilized Zirconia Electrolytes." ISS Transactions, 10, (1989), pp. 29-38.

24. D. Janke, "A New Immersion Sensor for the Rapid Electrochemical Determination of Dissolved Oxygen in Metallic Melts." Solid State Ionics, 3/4, (1981), pp. 599-604.

25. E.T. Turkdogan and R.J. Fruehan, "Review of Oxygen Sensors for Use in Steelmaking and of Deoxidation Equilibria." Canadian Metallurgical Quarterly, 11, (1972), pp. 371-382.

26. K.S. Goto, "Use of Oxygen Sensors for Steelmaking in Japan." Scandinavian Journal of Metallurgy, 12, (1983), pp. 43-44.

27. T. Tran and M.P. Brungs, "Application of Oxygen Electrodes in Glass Melts. Part 2. Oxygen Probes for the Measurement of Oxygen Potential in Sodium Disilicate Glass." Physics and Chemistry of Glass, 21, (1980), pp. 178-183.

28. D.S. Goldman, "Oxidation Equilibrium of Iron in Borosilicate Glass." Journal of the American Ceramic Society, 66, (1983), pp. 205-209.

29. E. Heikinheimo, "Iron Oxide Activity in Complex Silicate Slags." Solid State Ionics, 3/4, (1981), pp. 541-545.

30. C.B. Alcock and S. Zador, "Experimental Considerations in the Use of Solid Oxide Electrolytes." Canadian Metallurgical Quarterly, 13, (1974), pp. 321-323.

31. T. Tran and M.P. Brungs, "Application of Oxygen Electrodes in Glass Melts. Part 1. Oxygen Reference Electrode." Physics and Chemistry of Glass, 21, (1980), pp. 133-140.

32. K.C. Pun, "Assessment of Solid Electrolyte Sensor for Oxygen Potential Measurements of Submerged Arc Welding Fluxes", M.Eng. Thesis, University of Alberta, 1985.

33. A.V. Molodchikov, V.P. Luzgin and I.Z. Zinkovski, "Influence of Electronic Conductivity Component of $ZrO_2(Y_2O_3)$ on Accuracy of Oxygen Activity Determination in Liquid Steel." Steel in the USSR, 18, (1988), pp. 304-306.

34. Omega Engineering Inc., Temperature Measurement Handbook, Stanford, Connecticut, 1979.

35. JANAF Thermochemical Tables, 3rd Edition, Part II, Vol. 14, National Bureau of Standards, (1985).

36. M. Iwase, H. Akizuki, E. Ichise and Y. Tanaka, "Activities of Fe_xO in $CaO + CaF_2 + SiO_2 + Fe_xO$ Quaternary Slags by Disposable Electrochemical Oxygen Probes." Steel Research, 57, (1986), pp. 436-443.

37. D.J. Sosinsky and I.D. Sommerville, "The Composition and Temperature Dependence of the Sulfide Capacity of Metallurgical Slags." Metallurgical Transactions B, 17B, (1986), pp. 331-337.

APPENDIX A

SAMPLE CALCULATION OF OPTICAL BASICITY

The optical basicities of the fluxes were calculated using the following formula.

$$OB = X_1 OB_1 + X_2 OB_2 + X_3 OB_3 + \ldots$$

where OB is the optical basicity with $OB_{CaO} = 1$ and X is the equivalent cation fraction based on the fraction of negative charge neutralized by the charge of the cation concerned.

The values of OB for the components of the flux used to calculate the flux OB are based on the Pauling's Electronegativity and are as follows:

OXIDE	OB	MOLE % (Flux #1)
Na_2O	1.15	1.97
MgO	0.78	0.00
Al_2O_3	0.605	8.45
SiO_2	0.48	37.15
CaO	1.00	19.55
TiO_2	0.61	22.25
MnO	0.59	0.00
FeO	0.51	0.75
ZrO_2	0.69	0.29
CaF_2	0.80	9.02

For an example we take flux #1 whose composition based on mole percent is given above. The most convenient relation for X for each component is:

$$X = \frac{\text{(mole fraction of component)(total positive charge per molecule)}}{\Sigma\,\text{(mole fraction of component)(number of oxygen atoms per molecule)(2)}}$$

$$\text{Thus } X_{CaO} = 2*19.55 \,/\, (1.97 + 0 + 6*8.45 + 4*37.15 + 2*19.55 + 4*22.25 + 0 + 2*0.75 + 4*0.29 + 0)$$

$$X_{CaO} = 0.118$$

This calculation is repeated for each component of the flux and plugged into the optical basicity formula given above. The final optical basicity for this flux is:

OB (flux #1) = 0.616

APPENDIX B

SAMPLE CALCULATION OF ln pO_2

For a Pt-Mo thermocouple the EMF is (ref. 21):

$$E_T = -22.1 + 0.040\ T \quad (1)$$

where T is the temperature in Kelvin and E_T is the thermo-electromotive force in millivolts.

For a Pt-10Rh thermocouple the EMF is (ref. 34):

$$E_T = -5.374 + 0.012012\ T \quad (2)$$

A Pt-6Rh thermocouple EMF can be found by multipling the Pt-10Rh EMF by 0.6 to get:

$$E_T = -3.441 + 0.00721\ T \quad (3)$$

A Pt6Rh-Mo thermocouple is found by combining equations 1 and 3.

$$E_T = -18.7 + 0.033\ T \quad (4)$$

The oxygen probe EMF is related to the oxygen pressure by the following formula.

$$E = (RT/4F)\ (\ln pO_2(\text{flux}) - \ln pO_2(\text{ref})) + E_T \quad V \quad (5)$$

The ln pO_2(ref) for a Mo/MoO_2 reference is (ref. 35):

$$RT \ln pO_2 = -560369 + 160.037\ T \quad J/\text{mole } O_2 \quad (6)$$

The ln pO_2 for the flux can be calculated by substituting equations 4 and 6 into equation 5 and solving for ln pO_2(flux).

$$\ln pO_2(\text{flux}) = -68300/T + 20.8 + 46400\ E/T \quad (7)$$

For example at 1600 K an oxygen probe giving an EMF reading of 0.400 V would mean the flux has a ln pO_2 = -10.3.

APPENDIX C

SAMPLE CALCULATION OF PERCENT OXYGEN

For flux #1 the oxygen pressure was found from the data of this study to fit the following equation.

$$\ln pO_2 = 5.259 - 31150/T \quad \text{.....(1)}$$

The density of iron is 7.87 g/cm^3 and the density of the slag is approximated to be 2.5 g/cm^3. For a 1000 g sample of iron in which a equal volume of slag is melted the weight of slag melted would be:

$$\frac{1000 * 2.5}{7.87} = 317.7 \text{ g}$$

At 1800 K the ln pO_2 for flux #1 as calculated by equation 1 is -12.05, which is equal to a pO_2 of 5.845 X 10^{-6} atm. Asuming that pO_2 equals the mass fraction of oxygen in the flux which is available to the iron, the theoretical percent oxygen in the iron would be:

$$\text{percent oxygen} = \frac{\text{weight of oxygen available}}{\text{Total weight}} * 100$$

$$\%O = \frac{317.7 * 5.845X10^{-6}}{1000 + (317.7 * 5.845 X 10^{-6})} * 100 = 1.857 X 10^{-4} \%$$

APPENDIX D

RELATIONSHIP BETWEEN ln pO_2 AND FLUX CHEMISTRY

The weight percentages of the flux components were given in Table 5. Converting these over to mole percentages we get the following values.

	MOLE PERCENTAGES				
	#91	#20	#50	#1	#3
Na_2O	5.33	0.19	0.42	1.97	1.76
MgO	3.19	13.27	0.88	0.00	25.17
Al_2O_3	2.83	2.67	2.82	8.45	0.99
SiO_2	39.24	56.82	47.05	37.15	47.55
CaO	38.07	23.83	10.44	19.55	0.75
TiO_2	2.93	0.13	0.56	22.25	0.00
MnO	0.20	0.00	33.14	0.00	18.31
FeO	0.17	0.20	1.99	0.75	0.79
ZrO_2	0.00	0.00	0.00	0.29	0.00
CaF_2	7.94	2.84	2.33	9.02	4.62
ln pO_2(1600)	-20.53	-18.51	-9.10	-14.21	-7.98
ln pO_2(2600)	-2.77	-2.19	-1.53	-6.73	-6.17

The oxygen pressures were calculated from the least squares fit of ln pO_2 versus the inverse of temperature (1/T) using the data from this study. We can run a regression analysis with multiple variables using the calculated ln pO_2 as the dependent variable and the mole percentages as the independent variables. With five fluxes, a maximum of three independent variables can be used in a multiple regression analysis. Using the mole percentages of MnO, SiO_2 and (CaO + CaF_2) as the independent variables we get the following equation.

$$\ln pO_2(1600) = -0.327\ (CaF_2 + CaO) - 0.249\ SiO_2 + 0.073\ MnO + 4.322$$
$$r^2 = 1.000$$

Repeating the analysis at 2600 K gives us the equation,

$$\ln pO_2(2600) = 0.218\ (CaF_2 + CaO) + 0.259\ SiO_2 + 0.186\ MnO - 22.809$$
$$r^2 = 0.992$$

By repeating this calculation at several temperatures we find that the coefficients vary linearly with 1/T. In fact the coefficients must vary linearly with 1/T because the ln pO_2 for each flux varies linearly with 1/T. The values of these coefficients at any temperature can be found by interpolating between the values at 1600 K and 2600 K. They also can be represented by the following equations where

$$\ln pO_2 = A\,(CaF_2 + CaO) + B\,SiO_2 + C\,MnO + D.$$

$A = 1.0905 - 2268.7/T$
$B = 1.0717 - 2112.4/T$
$C = 0.3657 - 468.06/T$
$D = -66.219 + 112870/T$